

Blood & Heat

Morphology and Spreading Behavior of Blood Droplets Impacting an Inclined Pre-Heated Surface

Smart Solutions Semester

Mees Bouwman, Kuba Karkus, Mariëlle
Kortlever, Jimme Wolberink



Blood & Heat

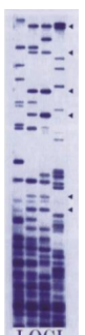
Morphology and Spreading Behavior of
Blood Droplets Impacting an Inclined
Pre-Heated Surface

by

Mees Bouwman, Kuba Karkus, Mariëlle
Kortlever, Jimme Wolberink

Tutors: J. Brons, N. Zeijen, E. Snippe, M. Steenhuisen
Cliënt: Loci Forensics B.V.
Cliënt tutors: M. Eversdijk, R. Gelderman
Project Duration: 01-09-2025 - 30-01-2026
Faculty: Life Science, Engineering and Design (LED), Enschede

Cover: "The physics of blood spatter", Physics World [26].



Preface

This project was carried out in collaboration with Loci Forensics B.V. The findings and recommendations on the behavior of blood on a heated surface are described in this work. The purpose of the experiments conducted in this report is to fill a research gap in the investigation of bloodstains. Four distinct temperatures are chosen that correspond to a particular boiling regime (excluding room temperature), at four different impact angles and three different drop heights (i.e., the impact velocity). All of these measurements will be conducted on the same surface to minimize influencing parameters.

For further information and a detailed overview of the authorship of each part of this document, please refer to Appendix F.

We are grateful to Nicole Zeijen, Esther Harzevoort, Jonathan Brons and Marten Steenhuisen for their support and guidance. Lastly, we would like to express our sincere appreciation for the assistance and expertise provided by Martin and René from Loci Forensics B.V.

Saxion, Enschede,

30–01–2026

Mees Bouwman	(Applied Physics student)
Kuba Karkus	(Forensic Investigation student)
Mariëlle Kortlever	(Forensic Investigation student)
Jimme Wolberink	(Archaeology student)

Samenvatting

Een samenvatting...

Summary

A summary...

Contents

Preface	i
Samenvatting	ii
Summary	iii
List of Figures	v
List of Tables	vii
Nomenclature	ix
1 Introduction	1
1.1 Goal and scope	1
2 Theory	3
2.1 Bloodstain Formation	3
2.1.1 Coagulation	3
2.1.2 Bloodstain patterns	3
2.1.3 Non-Newtonian properties of blood	4
2.2 Heat and Blood	4
2.3 Impact Angle	6
2.4 Drop Impact	6
2.4.1 Maximum spreading under inclined surfaces	7
3 Experimental Methods	9
3.1 Blood source and physical properties	9
3.2 Setup and the Experiment	9
3.3 Bloodstain appearance	12
3.4 Drop spread	12
3.5 Angle of impact and the W/L-ratio	14
3.6 Data analysis	15
4 Results and Interpretation	19
4.1 Effect of Temperature and Impact Angle Upon the Bloodstain Width, W	19
4.2 Blood impacts in different boiling regimes	20
4.3 Impact angle	25
4.4 Droplet spreading	26
5 Development New Experimental Setup	27
6 Discussion	28
7 Conclusion	29
8 Recommendations and Outlook	30
References	31
A Derivation of the Impact Velocity Using Bernoulli's Law	34
B Approximating an Ellipse given 4 corner points + MATLAB code translation	36
C Spread of Individual Impact Angle Measurements	41
D Bloodstain graphs	43
E Used equations	53

F Task Division**55**

List of Figures

2.1	Schematic of water droplets resting on a superhydrophobic, hydrophobic, and hydrophilic material.	3
2.2	Blood spatters in three different velocities. [forensicreader.com.]	4
2.3	A typical boiling curve of water (H_2O) at 1 atm, highlighting the boiling regimes: (A) natural convection (at around the room temperature), (B) nucleation-boiling regime, (C) transition-boiling regime, (D) film-boiling regime [31].	5
2.4	Effect of impact angle on bloodstain formation.	6
2.5	Different splashing behaviours and blood a droplet impact.	7
2.6	Schematic of drop impact droplet on an inclined surface.	8
3.1	Illustration of what could be a possible experimental setup to investigate the morphology and splashing behaviour of a blood droplet on an angled heated surface.	10
3.2	Ellipse fit of a bloodstain using our MATLAB script. The green outline represents the fitted ellipse, the red dots indicate the four points used for fitting, and the red cross marks the ellipses center. The stain shown was deposited on a ceramic surface at room temperature, photographed 45 seconds after impact, on a 60° inclined surface, from a drop height of 30 cm. The reference metric used in this figure is cut out for better illustration.	13
3.3	On the left, Equation 2.1 is plotted with the impact angle α (in degrees) on the x-axis and the W/L -ratio on the y-axis. On the right, the sensitivity function Equation 3.4 is shown. The shaded gray region ($75^\circ \leq \alpha \leq 90^\circ$) indicates the range in which Equation 2.1 becomes unreliable due to these amplified measurement errors.	14
3.4	An ellipse fitted to the bloodstain resulting in an underestimation of the angle of impact (incorrect fit) and the ellipse that should be measured (correct fit). The differences in the ellipses include the length and how well they fit the bloodstain at the leading edge.	15
3.5	Flowchart of the MATLAB script used for bloodstain analysis. The diagram outlines the full workflow. The results are stored in a table.	16
3.6	The spread of the measured impact angle at $\alpha = 60^\circ$ ($\theta = 30^\circ$) with three different drop heights. Each data point is an average of 3 blood drops ($N = 3$). It seems that the drop height (i.e. the impact velocity) does not affect the accuracy of the impact angle.	17
4.1	Maximum width (W_{\max}) as a function of temperature for three different heights (H).	19
4.2	Recorded pictures 45 seconds after impact of the passive drip stains on a specific surface temperature. In this figure the surface was at room temperature $\sim 23^\circ C$ (Repeat 2). Deformation of the stain increases with velocity (bottom to top) and with surface inclination (left to right).	20
4.3	Recorded pictures 45 seconds after impact of the passive drip stains on a specific surface temperature. In this figure the surface was heated to a temperature of $\sim 90^\circ C$ (Repeat 2). Deformation of the stain increases with velocity (bottom to top) and with surface inclination (left to right).	21
4.4	Recorded pictures 45 seconds after impact of the passive drip stains on a specific surface temperature. In this figure the surface was heated to a temperature of $\sim 120^\circ C$ (Repeat 2). Deformation of the stain increases with velocity (bottom to top) and with surface inclination (left to right).	22
4.5	Recorded pictures 45 seconds after impact of the passive drip stains on a specific surface temperature. In this figure the surface was heated to a temperature of $\sim 160^\circ C$ (Repeat 1). Deformation of the stain increases with velocity (bottom to top) and with surface inclination (left to right).	23

4.6 Recorded pictures 45 seconds after impact of the passive drip stains on a specific surface temperature. In this figure the surface was heated to a temperature of $\sim 230^{\circ}C$ (Repeat 2). Deformation of the stain increases with velocity (bottom to top) and with surface inclination (left to right).	24
4.7 Summary of blood droplet impact behavior on a heated surface shown within the classical boiling-curve regime of water. The images illustrate stain patterns of droplets impacting at a 30° angle from a drop height of 90 cm. As the surface temperature increases, the droplet morphology	24
4.8 Caption	25
4.9 Caption	25
4.10 Caption	26
A.1 Schematic of the drop impact situation.	34
C.1 The spread of the measured impact angle at $\alpha = 30^{\circ}$ ($\theta = 60^{\circ}$) with three different drop heights. Each data point is an average of 3 blood drops ($N = 3$). It seems that the drop height (i.e. the impact velocity) does not affect the accuracy of the impact angle.	41
C.2 The spread of the measured impact angle at $\alpha = 75^{\circ}$ ($\theta = 15^{\circ}$) with three different drop heights. Each data point is an average of 3 blood drops ($N = 3$). It seems that the drop height (i.e. the impact velocity) does not affect the accuracy of the impact angle.	42
C.3 The spread of the measured impact angle at $\alpha = 90^{\circ}$ ($\theta = 0^{\circ}$) with three different drop heights. Each data point is an average of 3 blood drops ($N = 3$). It seems that the drop height (i.e. the impact velocity) does not affect the accuracy of the impact angle.	42
D.1 Recorded pictures 45 seconds after impact of the passive drip stains on a specific surface temperature. In this figure the surface was $\sim 23^{\circ}C$ (Repeat 1).	43
D.2 Recorded pictures 45 seconds after impact of the passive drip stains on a specific surface temperature. In this figure the surface was $\sim 23^{\circ}C$ (Repeat 3).	44
D.3 Recorded pictures 45 seconds after impact of the passive drip stains on a specific surface temperature. In this figure the surface was $\sim 90^{\circ}C$ (Repeat 1).	45
D.4 Recorded pictures 45 seconds after impact of the passive drip stains on a specific surface temperature. In this figure the surface was $\sim 90^{\circ}C$ (Repeat 3).	46
D.5 Recorded pictures 45 seconds after impact of the passive drip stains on a specific surface temperature. In this figure the surface was at room temperature $\sim 120^{\circ}C$ (Repeat 1).	47
D.6 Recorded pictures 45 seconds after impact of the passive drip stains on a specific surface temperature. In this figure the surface was at room temperature $\sim 120^{\circ}C$ (Repeat 3).	48
D.7 Recorded pictures 45 seconds after impact of the passive drip stains on a specific surface temperature. In this figure the surface was heated to a temperature of $\sim 160^{\circ}C$ (Repeat 2).	49
D.8 Recorded pictures 45 seconds after impact of the passive drip stains on a specific surface temperature. In this figure the surface was heated to a temperature of $\sim 160^{\circ}C$ (Repeat 3).	50
D.9 Recorded pictures 45 seconds after impact of the passive drip stains on a specific surface temperature. In this figure the surface was heated to a temperature of $\sim 230^{\circ}C$ (Repeat 1).	51
D.10 Recorded pictures 45 seconds after impact of the passive drip stains on a specific surface temperature. In this figure the surface was heated to a temperature of $\sim 230^{\circ}C$ (Repeat 2).	52

List of Tables

3.1	Physical parameters of (human)blood at $37^{\circ}C$ (Body temperature).	9
3.2	Impact velocity V_0 as a function of release height h , measured from the pipette tip to the impacting surface. Calculated using Equation 3.1. Measurement error margins are omitted because the applied equation systematically overestimates the true impact velocity.	11
3.3	Validation of the pipette setting of $15 \mu\text{L}$. Blood droplet mass measurements are reported as mean values with their corresponding 95% confidence intervals. The mean and standard deviation were calculated from three independent mass measurements of blood droplets.	11
3.4	Overview of Measurement Parameters and Indexing	16
F.1	Distribution of the workload	55
F.2	Table with a summary of all the roles and tasks.	56

Nomenclature

Abbreviations

Abbreviation	Definition
BPA	Blood Spatter Analysis
CT	Clotting Time
Defibrinated blood	Blood from which fibrin has been removed, preventing clotting
Re	Reynolds number, ratio of inertial to viscous forces in a fluid
Satellites	Smaller droplets that break away from the main droplet upon impact
Spines	Radial, finger-like projections around the edge of a bloodstain
We	Weber number, ratio between capillary and inertial forces in a fluid
Leidenfrost effect	Formation of a vapor layer allowing a droplet to levitate on a hot surface

Symbols

Symbol	Definition	Unit
D_0	Initial droplet diameter	[m]
T_b	Boiling point of blood	[°C] or [K]
T_d	Droplet temperature	[°C] or [K]
T_w	Surface (wall) temperature of the ceramic tile	[°C] or [K]
V_0	Impact velocity of the droplet	[m/s]
V_{\perp}	Normal velocity component relative to the inclined surface	[m/s]
α	Impact angle of the droplet	[°]
θ	Inclination angle of the surface	[°]

1

Introduction

The police were called in Mexico City for a fire in an apartment. After the firemen had extinguished the fire, the police started their investigation. Immediately after starting the examination of the place, a young male was found. The time of death was found to be approximately during the fire. Meaning, blood patterns could be left behind while room temperature increased due to the fire. Little to no discussion is known regarding this specific topic. The police were not able to draw any conclusions based on the bloodstains. This is a case example to illustrate why the research in this project could help in future investigations.

In forensic cases, the environment in which blood is deposited plays a crucial role [30, 27]. Especially hot temperatures and hot surfaces are interesting, as these can alter the appearance and composition of blood [3], making it difficult to understand how bloodstains were formed. After being exposed to high temperatures, blood may behave differently, it may dry out quickly or perhaps even become partially charred. Due to lack of information on the behavior of blood on heated surfaces, it is nowadays not possible to draw any certain conclusions.

Therefore our project is focused on how blood reacts while interacting with hot surfaces. The blood is being deposited from different heights and angles, whilst adjusting the temperature of a hot surface.

1.1. Goal and scope

The aim of this project is to investigate how different surface temperatures influence the morphology of a blood droplet under varying impact velocities and angles. To achieve that we:

- Develop an experimental setup that can simulate an environment with temperatures significantly higher than the boiling point of blood.
- Experimentally investigate how the morphology of a blood droplet are influenced by:
 - Variations in surface temperature (23 (room temperature), 90, 120, 160 and 230 °C).
 - Variations in inclination angle (0°, 15°, 30°, and 60°).
 - Variations in velocity, by releasing the droplet from different heights (30, 60, and 90 cm).

To help reach the main goal, other topics will be studied to help answer the main question. (1) First the impact angle of the droplets will be examined and compared with the theoretical ratio of impact angle to width/length. (2) After that the speed will be studied and compared to a theoretical line just like in the previous point. (3) Lastly The difference in appearance of the bloodstain will be described and how it possibly is changing due to a increase in surface temperature.

Hypothesis 1

At higher surface temperatures ($\geq 100^\circ$), the splashing behaviour of a blood droplet is expected to intensify. This is assumed because by increasing the temperature, the evaporation rate goes up as

well. The rapid formation of gas bubbles than weakens the surface tension, destabilizing the droplet which causes the droplet to splash, creating spines and satellites.

Hypothesis 2

As the surface angle increases less energy of the droplet is further given to the surface itself, this will mainly happen after the angle exceeds 45° . As a result, the drop than slides down in an elliptical form and spreads the impact energy, which is equal to the kinetic energy on impact, over a larger area. This way the energy is less put in spattering. At higher impact velocities, however, the kinetic energy increases with the square of the velocity, so splashing is expected to intensify, independent of the impact angle.

Hypothesis 3

Whilst the temperature increases the clotting of blood will happen faster, this will lead to a define ellipse being formed with clear border lines which will make the recognizing of that ellipse easier. Because of that define ellipse the calculation made afterwards will be more accurate and valid.

To help and test the described hypotheses an experiment has been designed where the surface is pre-heated. The slope of the surface is adjustable so different angles can be measured. As well as the slope the height from which the blood droplet is being dropped can be adjusted. These three variables, surface temperature, angle and height were chosen based on a research gap. After the measurement have been done the data will be analysed and calculation will be made. With clear results a conclusion can be drawn. This will lead to recommendations for future research, based upon mistakes and results

This report is organized as follows:

Chapter 2: Theory In this chapter the relevant theoretical and background information will be clarified. Firstly the bloodstain formation will be described, as well as what is so far been research on heat and blood. After that the theory of how impact angles and drop impact work will be discussed.

Chapter 3: Experimental Methods This chapter starts of with some blood properties and a schematic picture of the used setup. After that the velocities and the drop spread were calculated. Lastly in this chapter will be described what the angle of impact was and how the data analysis was performed.

Chapter 4: Results and Interpretation This chapter shows the results of the experiment and the interpretation of those. At the end of the chapter an error analysis is written out.

Chapter 6: Discussion Discussion stands for what has gone wrong and which imperfections could lead to wrong or invalid conclusions being drawn.

Chapter 7: Conclusion Here the conclusion has been drawn. The main question has been answered, as well as the side questions.

Chapter 8: Recommendations and Outlook Lastly, in this chapter recommendations for further research will be stated.

2

Theory

2.1. Bloodstain Formation

2.1.1. Coagulation

The coagulation or clotting of blood, can start in two ways: through the extrinsic or intrinsic pathway [5]. The extrinsic pathway is activated by a tissue factor released at site of injury via external trauma [24]. The intrinsic pathway is started in response to internal trauma [2]. These two pathways contain a cascade of events that will eventually lead to blocked blood flow inside the body[5].

Since this project focuses on the clotting of blood outside the body, it is important to know how this differs from inside the body. In the case of blood leaving the body, it being ex vivo, it will start to clot and dry [15, 4]. The fibrin strands are formed, creating a clot. After this, the water will start to evaporate to dry the clot out, until only a solid structure remains, consisting mainly of red blood cells. An important parameter for drying is the contact angle (Fig. 2.1) at which the blood will hit a surface. A smaller angle means covering a larger surface area for the blood to spread over, causing it to dry faster [15].

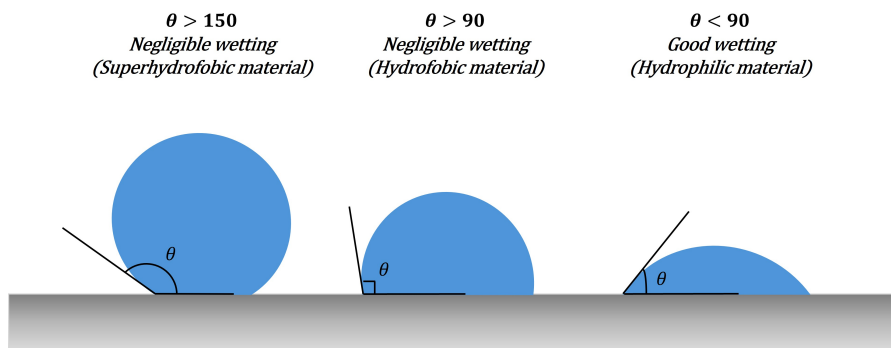


Figure 2.1: Schematic of water droplets resting on a superhydrophobic, hydrophobic, and hydrophilic material.

2.1.2. Bloodstain patterns

The classification of bloodstains can be done based on the correlation between the velocity of the drop and the size or diameter of the bloodstain [29]. Three categories are used:

Low-Velocity Impact Blood Spatter

These bloodstains are created when the blood is subjected to a force with a velocity up to 1.5 m/s. The stains usually are 4 mm in diameter or larger [29, 17] A higher velocity causes the stains to be smaller, as the force breaks the blood into smaller droplets.

Medium-Velocity Impact Blood Spatter

Medium-Velocity Impact Blood Spatters are created when the source of blood is subjected to a force with a velocity between 1.5-7.6 m/s. The resulting stains are in the size range of 1-3 mm. Stains in this category are usually associated with beatings and stabbings [29, 8].

High-Velocity Impact Blood Spatter

These bloodstains are created when the blood is subjected to a velocity up to 30 m/s. The stains are generally smaller than 1 mm in size and are associated with gunshot injuries [29].

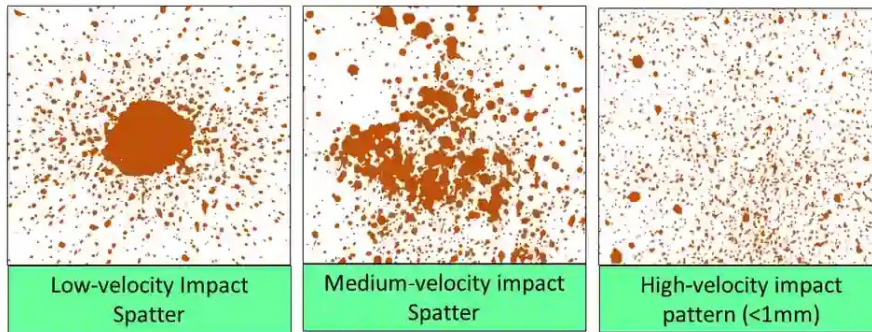


Figure 2.2: Blood spatters in three different velocities. [forensicreader.com.]

2.1.3. Non-Newtonian properties of blood

Nog niet af

2.2. Heat and Blood

Bloodstains are mostly encountered on crime scenes involving violence, sometimes those crime scenes are set on fire. The fire makes the temperature rise and it is often difficult to detect blood. Due to blood's intense red colour it's easily made visible on a lot of backgrounds, however the walls for example become very dark after exposure to fire. That makes detecting bloodstains a lot harder. There are little to no published scientific articles about this topic, so it is a fairly new branch in the field of forensic science in the context of BPA [3]. However, there is a significant amount of research done on the effects of water droplets and other liquids on a heated surface [37, 23, 31]. Much of this research has been done analytically or carried out using high-speed cameras combined with experiments for analyzing the droplet's rebound and its behaviour when heated [11].

According to Gregg et al. [10], blood consists of approximately 50% water, along with various cell molecules. The paper clearly notes that there is some uncertainty regarding the exact percentage of water in a blood droplet. The 50% estimation is based on the findings of Marieb and Hoehn (2010) [19], who stated that blood consists of approximately 55% blood plasma and 45% erythrocytes. If 55% of blood is plasma and 90% of plasma consists of water, then blood should contain 49.5% water (rounded to 50%). The only way to know exactly what the water content is by drying a single droplet and comparing its weight before and after drying. Hypothetically, this method should give the exact water percentage of a blood droplet.

It should be noted that the water percentage here is not necessarily the standard for all blood droplets. The water content of a healthy individual may differ from that of a person with a blood disorder or other conditions that affect the water consistency of blood. Therefore, in the ideal case, a fresh blood sample from the victim is needed to accurately determine the water composition of the blood [10].

The water content of blood plays a crucial role in the morphology of blood drops on heated surfaces. Since blood consists approximately of 50% water, the typical boiling curve of water at 1 atm depicted in Figure 2.3, can then be used to interpret the different temperatures that blood is exposed to when impacting a heated surface. This is shown by the surface heat flux as a function of excess temperature, expressed by $\Delta T_{excess} = T_s - T_{sat}(^{\circ}C)$ where T_s is the surface temperature and T_{sat} is the saturation temperature; in the case of water, T_{sat} is equal to $100^{\circ}C$. The boiling curve is described in

four different well-studied regimes corresponding to (A) natural convection, (B) nucleation-boiling, (C) transition-boiling, and (D) the film-boiling regime.

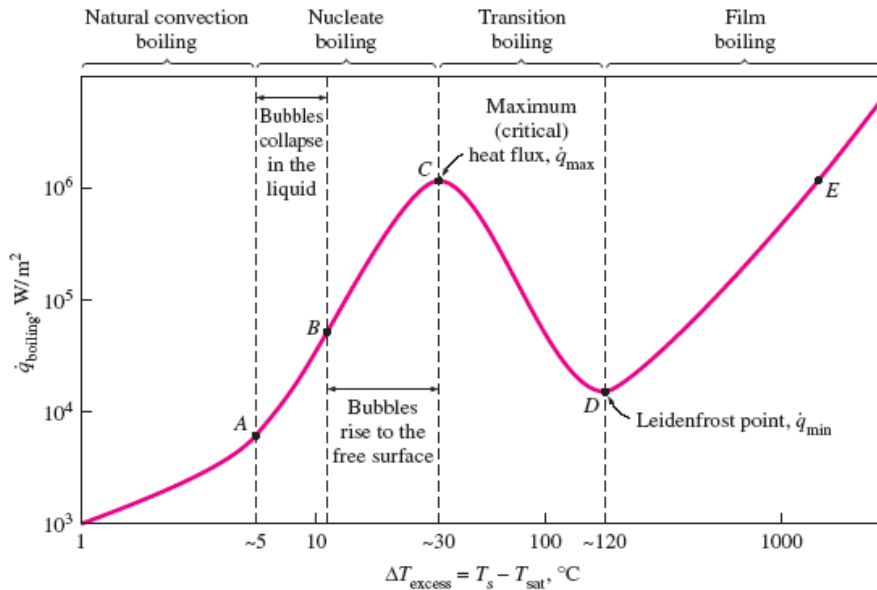


Figure 2.3: A typical boiling curve of water (H_2O) at 1 atm, highlighting the boiling regimes: (A) natural convection (at around the room temperature), (B) nucleation-boiling regime, (C) transition-boiling regime, (D) film-boiling regime [31].

The natural convection regime, shown in section (A) on Figure 2.3, involves natural heat flow and temperatures of around $22^\circ C$ (room temperature) to just below the boiling point of water and blood (around $100^\circ C$ for both fluids). In this phase, there is a steady increase of the fluid volume, due to the expansion and excitation of the molecules. Nucleate boiling, shown in section (B), is when bubbles are starting to form and rise. This stage is divided in two separate stages, firstly where bubbles start to form at various places and collapse in the liquid itself. In the second stage, bubbles reach the liquid surface where they collapse, causing vapor release and begins to evaporate. When transition boiling starts, shown in section (C), the fluid starts to evaporate more rapid due to higher temperatures.

Lastly, in the film boiling regime, the Leidenfrost effect becomes significant. This region is particularly important in a forensic context. This is where the surface temperature is significantly hotter than the liquid's boiling point, in this case for blood the boiling point is approximately $120^\circ C \leq \Delta T_{excess}$ [16]. When a drop of blood strikes the heated surface, a thin layer of vapor instantly forms between the drop and the heated surface preventing the drop to make contact with the surface. This why the blood drop starts to skid all around the place.

In the paper of Larkin et al. (2013)^[16] were extensive experiments performed regarding these four boiling regimes with blood droplets, this was a follow up the research done by Lee Hulse-Smith et al. (2005)^[12] which only looked at the bloodstain characteristics at room temperature. Larkin et al. (2013)^[16] found that there is a distinct pattern in bloodstain diameters, where bloodstain diameters experience an increase up to temperatures of $90^\circ C$ and then subsequently decrease at a parallel rate as the temperature increases, suggesting a steady evaporation. Therefore, the four previously discussed boiling regimes of water can be applied to blood, only at slightly higher temperatures. During these regimes, changes of the final bloodstain appearance were observed, different rings are formed due to the separation of blood in its components. A correlation was found between height, thus initial velocity V_0 , where the blood drops are released from, and the number of rings, where lower heights produced fewer rings.

In the study of Lee Hulse-Smith et al. (2005)^[12], an analytical solution developed by Mehdizadeh et al.^[21] was used to predict the number of spines. The experimental results were consistent with this analytical solution. In contrast, Larkin et al. (2013)^[16] reported that “*the number of spines deemed insignificant when blood is dropped on to a heated surface, there appearance becomes sporadic and does not follow any general pattern*”. They further suggest that satellite spatter might serve as a substitute for the

spines, as it was observed that the number of satellites increased with rising temperatures. However, this claim has not yet been validated or disproven. In this research, this hypothesis will not be looked at.

2.3. Impact Angle

Bloodstains are almost always elliptical (Fig. 2.4), depending on the impact angle (α). The only case a bloodstain is circular, is when α equals 90° , otherwise its elliptical. In addition, they often have a tail showing the direction of travel of the original blood droplet, which is generally quantified by the directional angle γ the bloodstain has compared to the vertical of the surface/wall.

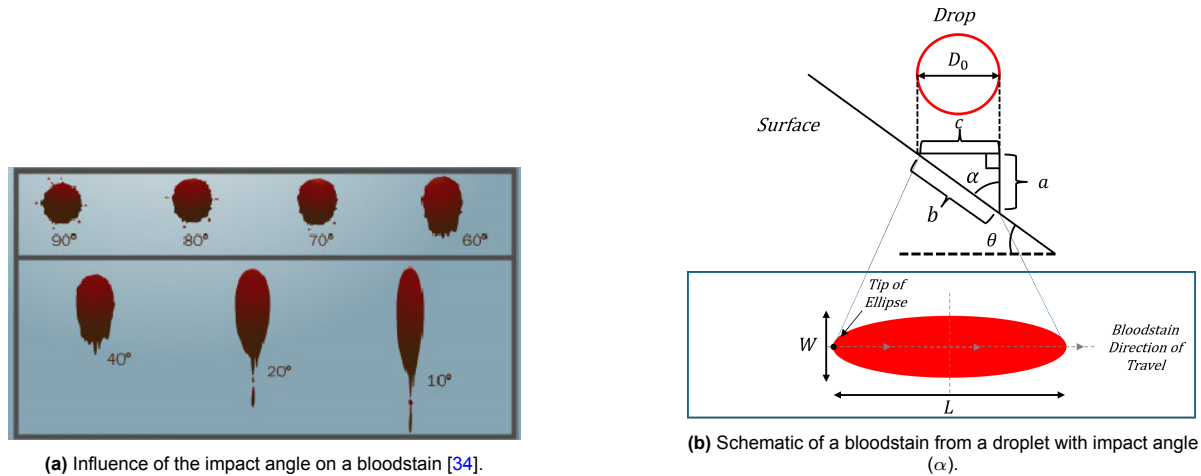


Figure 2.4: Effect of impact angle on bloodstain formation.

A picture perpendicular of the bloodstain can be taken, which than is used to determine the impact angle (α), which is directly related to the elliptical shape of the bloodstain given by the following [1]:

$$\sin \alpha = (W_{max}/L_{max}) \quad (2.1)$$

When the final stain comes to rest, the stain tends to be more elongated in the length to accurately determine the impact angle due to the inertia of the excess fluid that did not stick to the surface. This effect also explains the formation of the characteristic tail. To correct for this elongation, an ellipse is typically fitted to the leading edge of the stain, i.e., only the upper half of the stain is used as the reference for the ellipse fitting. From this fitted ellipse, the maximum length (L_{max}) and width (W_{max}) are obtained, which are then used to determine the impact angle using Equation 2.1.

2.4. Drop Impact

The field of study related to blood drop stains in forensic applications falls nowadays in the large topic that is the impact of complex fluid droplets. There is extensive research done on Newtonian-fluids such as water droplets [9]. Different splashing behaviours were observed and studied in the last century, these behaviours are classified as the following: deposition, corona splash, prompt splash, receding break-up, and partial or full rebound as shown in Figure 2.5a, from the review of Marengo et al. [18].

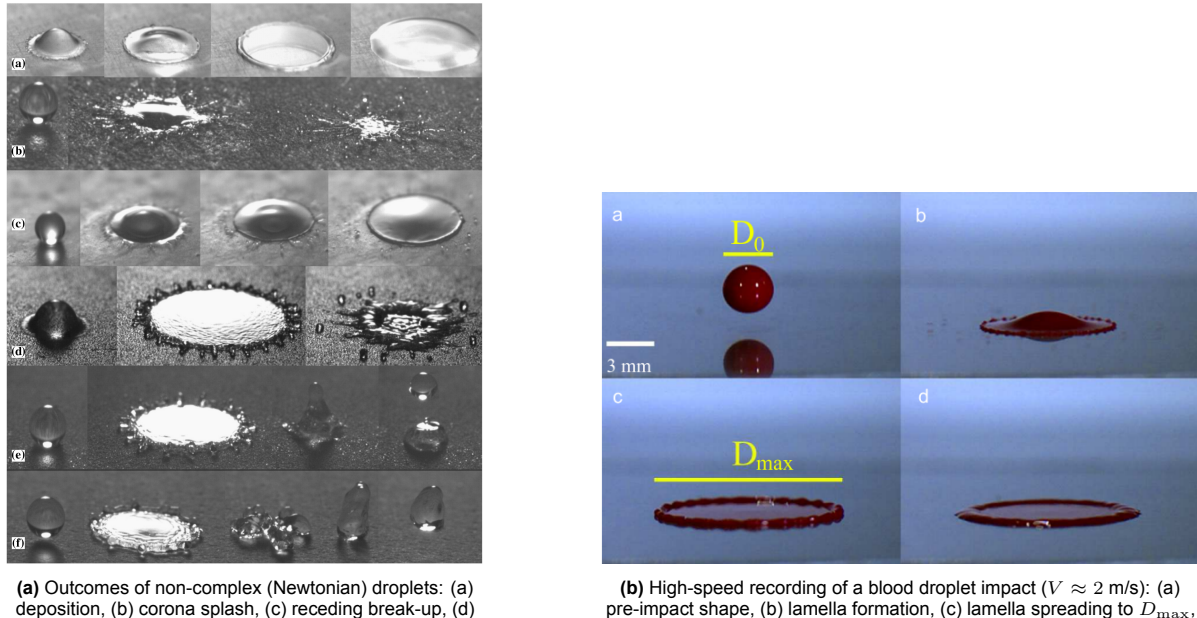


Figure 2.5: Different splashing behaviours and blood a droplet impact.

When a droplet hits the surface, it rapidly spreads in a circle within several milliseconds, as observed in Figure 2.5b. The spreading and different splashing behaviours are mainly driven by the inertia of the droplet, and countered by the capillary and viscous forces [20, 28]. Other parameters, such as gravity, impact velocity, impact angle, surface roughness, and initial droplet diameter, also play a crucial role in how a liquid deforms when impacted on a hard surface.

In general, the inertial, capillary, and viscous forces are quantified in terms of the ratio between the inertial and capillary forces, i.e., the Weber number:

$$We = \frac{\rho D_0 V_0^2}{\sigma} \quad (2.2)$$

or between the inertial and viscous forces, i.e., the Reynolds number:

$$Re = \frac{\rho D_0 V_0}{\mu} \quad (2.3)$$

where D_0 is the initial drop diameter, V_0 the impact velocity, μ is the viscosity, ρ is the density, and σ denotes the liquid/air surface tension.

After a few milliseconds, the impacting droplet reaches its maximum diameter (D_{\max}). In forensics, the relationship between impact velocity and stain size (D_{\max}) is essential for properly analyzing bloodstain patterns, particularly for the trajectory reconstruction of a ballistic droplet [14]. The spreading factor is defined as the ratio between maximum and initial diameter (D_{\max}/D_0).

2.4.1. Maximum spreading under inclined surfaces

In the work done by Laan et al. (2015)^[14] it is demonstrated that a universal relation exists for general fluid spreading, including blood droplets, given by Equation 2.4:

$$\frac{D_{\max}}{D_0} \cdot Re^{-1/5} = \frac{P^{1/2}}{A + P^{1/2}} \quad (2.4)$$

Their work shows that the impact and spreading behavior of fluids on solid substrates in both the capillary and viscous regimes can be captured solely by energy conservation. This new model accurately predicts impact velocity from maximum spreading (D_{max}) by numerically solving Equation 2.4.

In Equation 2.4, the parameter P , referred to as the *impact parameter*, is defined as

$$P = We Re^{-2/5}.$$

The constant A is a fitting parameter, with a value of

$$A = 1.24 \pm 0.01.$$

On inclined surfaces, the length of the elliptical bloodstain is often longer than the ideal length. Therefore choosing the width (W_{max}) as the relevant parameter for the maximum spreading is more favorable.

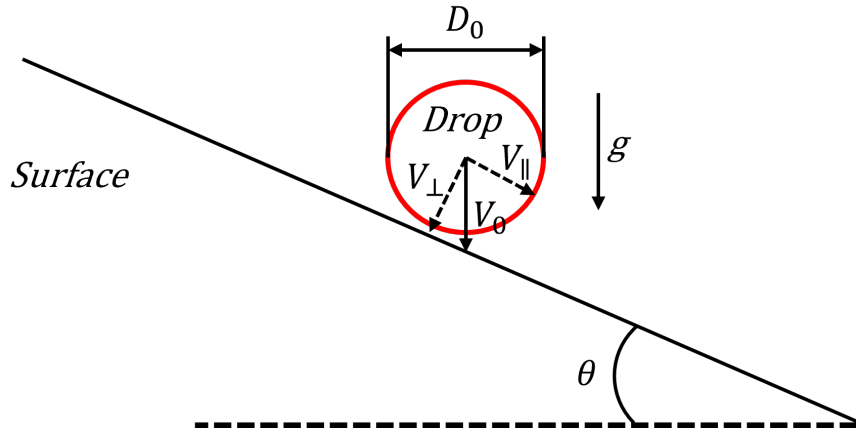


Figure 2.6: Schematic of drop impact droplet on an inclined surface.

The impact velocity can be divided, as seen in Figure 2.6, into a parallel and a perpendicular component with respect to the inclined surface, $V_\parallel = V_0 \cos \alpha$ and $V_\perp = V_0 \sin \alpha$, respectively. For spreading along the width only the perpendicular component of the impact velocity is taken into account. With that, Equation 2.4 can be rewritten as:

$$\frac{W_{max}}{D_0} = Re^{1/5} \cdot \frac{P^{1/2} \sin \alpha}{(A + P^{1/2}(\sin \alpha)^{4/5})} \quad (2.5)$$

To date, no research has been conducted on the impact patterns of blood on both heated and angled surfaces. Our interest is therefore focused on: bloodstain patterns, a non-Newtonian fluid, impacting an angled heated surface on a non-porous ceramic tile.

3

Experimental Methods

3.1. Blood source and physical properties

The blood used to perform the experiments was defibrinated sheep blood. Defibrinated stands for blood from which the fibrin protein has been removed. Fibrin is responsible for clotting, the absence of it means that blood can not clot on its own and is suitable for various applications [6]. Thermo Fisher Diagnostics B.V. (Netherlands), manufactured by TCS Biosciences Ltd (UK) was the supplier of the blood used during this project.

Blood has many functions inside a human body. For instance transport of nutrients and oxygen, as well as absorption. There are three main properties of blood when it comes to blood flow, which is relevant in these experiments [32].

Firstly, the viscosity, which is influenced by many parameters. The amount of red blood cells and the viscosity of the plasma itself directly influence it. Plasma contains long proteins which are a big factor when calculating or measuring the viscosity of blood [22].

The density of blood is another crucial property which influences how the blood will behave when dropped on a surface. Density varies depending on weight, age and gender, but also the species. Blood has a density a bit higher than water mostly due to the presence of proteins and red blood cells [25].

Lastly, the surface tension of blood. This property is important because it has proven influence on how blood behaves and flows [36]. In the following the table the estimated values of the physical properties of blood are listed. Due to lack of information on sheep blood, it is assumed that these values are approximately the same for sheep blood and stay constant.

Table 3.1: Physical parameters of (human)blood at $37^{\circ}C$ (Body temperature).

Parameter	Value	References
Density blood, ρ [kg/m^3]	1063.56	[35]
Surface tension blood/air, σ [N/m]	$5.241 \pm 0.262 \cdot 10^{-2}$	[35]
Viscosity blood, μ [$\text{Pa}\cdot\text{s}$]	$3.352 \pm 0.360 \cdot 10^{-3}$	[35]

3.2. Setup and the Experiment

To investigate the influence of surface temperature, inclination, and impact velocity on bloodstain morphology and impact dynamics, we let defibrinated sheep blood drops impact a ceramic tile with controlled temperature and inclination. An overview of the entire setup is shown in Figure 3.1. In the experiments, the impact velocity V_0 , surface temperature T_w , and surface inclination θ were varied.

In dimensionless form, the control parameters are the Reynolds number $Re = \rho D_0 (V_0 \sin \alpha) / \mu$ and the Weber number $We = \rho D_0 (V_0 \sin \alpha)^2 / \sigma$. Our goal was to measure the dimensionless drop spread W_{\max}/D_0 , determine the impact angle α ($\theta = 90 - \alpha$), and make new observations regarding bloodstain appearance.

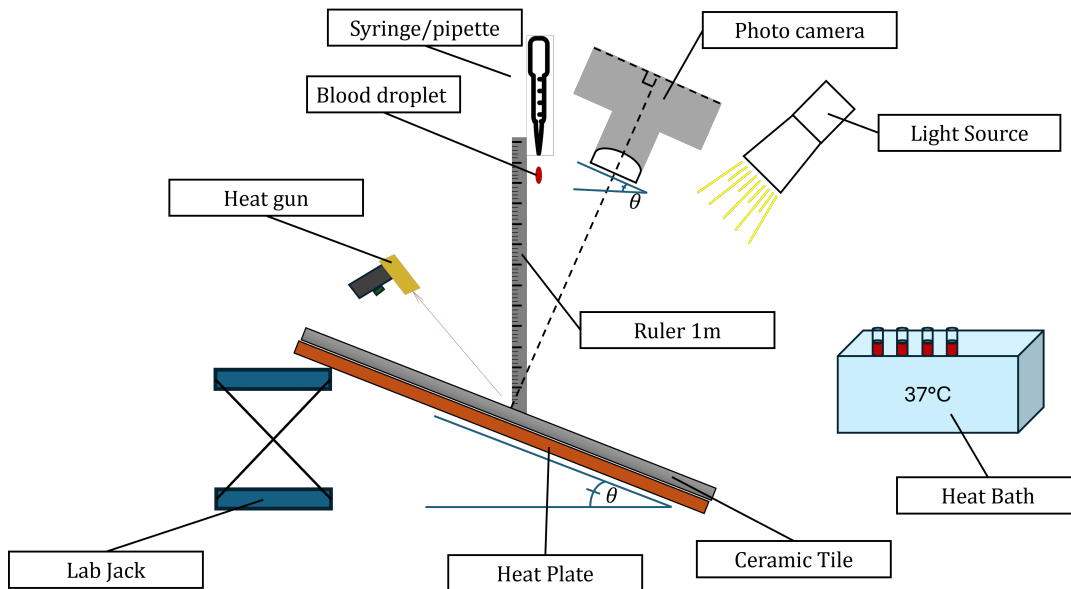


Figure 3.1: Illustration of what could be a possible experimental setup to investigate the morphology and splashing behaviour of a blood droplet on an angled heated surface.

Four different surface temperatures were selected, each corresponding to a distinct boiling regime (Fig. 2.3). For natural convection boiling, a temperature of 90°C was chosen, nucleate boiling 120°C, transition boiling 160°C, and for film boiling 230°C. A margin of $\pm 10^\circ\text{C}$ was applied to ensure that, in the most extreme cases, drops were not deposited in an unintended boiling regime. Additionally, a reference measurement was conducted at room temperature, approximately 21°C. By selecting surface temperatures that represent distinct boiling regimes, the resulting bloodstain appearance can be directly linked to the corresponding regime.

A non-porous matt white, wall ceramic tile (15x15 cm, 0.6 cm thick, supplier Max4Home) was used as the substrate for experiments in the temperature range 23°C - 160°C. Only two identical tiles were available, and both unfortunately fractured during the 230°C experiments due to the extreme heat. Therefore, a different type of ceramic tile had to be used for the measurements at 230°C. #### A heating plate (IKA C-MAG HS7 digital) was used to heat the ceramic tile to the desired temperature. The plate operates within a temperature range of 50°C–500°C with a resolution of 1 K, and has a heating surface of 21.5x33 cm. Test measurements showed that the heating was not perfectly homogeneous over the entire heating area, with the highest temperatures mostly near the center of the plate. To verify that the ceramic tile reached the intended temperature, an infrared thermometer (...) with an accuracy of $\pm 1.5^\circ\text{C}$ was used for monitoring.

The heated surface was inclined by placing a lab jack under one end of the heating plate. To verify that the intended angle was reached after adjusting the height of the lab jack, an analog angle gauge from the (...) manufacturer was used. In total, four different impact angles α were investigated: 90°, 75°, 60°, and 30° (corresponding to $\theta = 0^\circ, 15^\circ, 30^\circ$, and 60°).

A range of three different release heights was used to create varying impact velocities V_0 , as expressed in Table 3.2, and were calculated using Equation 3.1:

Table 3.2: Impact velocity V_0 as a function of release height h , measured from the pipette tip to the impacting surface. Calculated using Equation 3.1. Measurement error margins are omitted because the applied equation systematically overestimates the true impact velocity.

Release height h (cm)	Impact velocity V_0 (m/s)
30	2.43
60	3.43
90	4.20

$$V_0(h) = \sqrt{2gh} \quad (\text{Bernoulli/conservation of energy}) \quad (3.1)$$

where g is the acceleration due to gravity and h is the release height, measured from the pipette tip to the impacting surface using a regular meter ruler. The pipette was manually raised and held at the measured height. With this method, giving a small initial velocity to the droplet cannot be ruled out.

The impact velocity (V_0) is derived using simple fluid dynamics¹. This equation uses a few assumptions. The most relevant are: no air resistance (which is not true and definitely plays a role in the fall of a small droplet, but can be neglected with small velocities), initial velocity is zero, and pressure stays constant. With these assumptions, the calculated impact velocity overestimates the 'real' impact velocity ($V_{real} < V_{calculated}$). Therefore, throughout the remainder of this report, the impact velocity is corrected by applying a factor of 0.82 to the calculated velocity, and error bars involving the impact velocity are not shown. Due to problems operating the high speed camera, it was not possible to perform any kind of measurements using the high speed camera.

All the blood drop tests were performed by the same analysts throughout the study to ensure more consistent results. A micropipette fitted with a $15 \mu\text{L}$ tip nozzle with an inner diameter of 0.5 mm was used. The droplet volume (\mathcal{V}) produced by the pipette was determined from the mass of three independent blood droplets. The mean mass was multiplied by the fluid density (ρ) to obtain the volume, as detailed in Table 3.3, and therefore validating the indicated volume by the manufacturer (the micropipette corrects for left over residue in the tip nozzle). The corresponding droplet diameter was then calculated using Equation 3.2. Drops of size 3.06 ± 0.07 mm were generated using the micropipette.

Table 3.3: Validation of the pipette setting of $15 \mu\text{L}$. Blood droplet mass measurements are reported as mean values with their corresponding 95% confidence intervals. The mean and standard deviation were calculated from three independent mass measurements of blood droplets.

Property	Symbol	Value
<i>Mass</i>		
Average Mass	m	$15.93 \pm 1.01 \text{ mg}$ $(1.59 \pm 0.10) \times 10^{-5} \text{ kg}$
<i>Volume</i>		
Calculated from mass	\mathcal{V}_{calc}	$14.98 \pm 0.95 \mu\text{L}$
Pipette setting	\mathcal{V}_{set}	$15.0 \mu\text{L}$

$$\mathcal{V} = \frac{4}{3}\pi \left(\frac{D_0}{2}\right)^3 \Rightarrow D_0 = \left(\frac{6\mathcal{V}}{\pi}\right)^{1/3} \quad (3.2)$$

After a blood droplet was deposited on the substrate, the resulting elliptical bloodstains were photographed immediately after impact, and a second photograph was taken after 45 seconds. All images were captured using a Sony 4K Exmor R5 Cybershot camera positioned perpendicular to the surface to avoid induced parallax errors in the measurements.

¹In Appendix A, the full derivation is given for the impact velocity.

Each complete measurement set consisted of 60 measurements. Due to the large number of measurements and the limited available time, only three repeats were performed. In total, 180 blood droplets were deposited and 360 photographs were taken.

For each temperature, 12 measurements were conducted to cover all parameter combinations, resulting in 36 measurements when including the three repeats. These photographs were later used for the analysis.

3.3. Bloodstain appearance

The appearance of the bloodstains differs from each other due to variables used, such as drop height, surface angle, and surface temperature . To distinguish between differences in appearance, attention was paid to the presence of the following physical attributes:

- Blood plasma on the upper side
 - Some droplets slide down the surface, mostly consisting of only the red blood cells. The plasma is left behind at the place of impact. The plasma is a lighter-colored fluid, almost transparent.
- One big bubble in the middle
 - After droplets fall on the surface and start drying out, sometimes a bubble appears in the middle of the bloodstain, growing upwards.
- Multiple smaller bubbles
 - If the surface is above a certain temperature, the blood will start boiling as soon as it hits the surface, thus creating small bubbles.
- Clear color gradients on the upper side
 - The droplets slide down the surface, usually only leaving plasma behind. Sometimes red blood cells are also left, creating a gradient of plasma fluid, plasma mixed with some red blood cells and the bloodstain itself.
- A satellite on the bottom
 - At higher surface inclinations, the droplets tend to create a satellite at the bottom of the bloodstain.
- The blood stain is deep red
 - At lower temperatures, the blood stain will not be heated enough to turn a color as the result of burning. The bloodstain will stay its original color.
- The blood stain is brown
 - The blood stain will start cooking and burning at higher temperatures, causing the color to change to a more brown.

These attributes were used to create a table and categorize the photos of the blood droplets.

3.4. Drop spread

The resulting elliptical bloodstain dimensions after impact, with the minor axis as the width W and the major axis as the length L , are measured by taking photographs 45 seconds after impact using a reference metric for calibration. These photographs are analyzed with a self written MATLAB-script by fitting an ellipse manually using the four corner points². The ellipses were fitted along the leading edge of the stain while excluding obvious edge distortions, spines, and tails from the area of the ellipse (Fig. 3.2). For size calibration, four individual lines were drawn along a reference metric for each measurement. The mean of these four lines was then used for calibration, resulting in a mean standard deviation of ± 0.2 pixels per mm for the measured calibration lengths.

²In Appendix B, the mathematical derivation and the MATLAB-code translation for fitting an ellipse given the four corner points of the ellipse is provided.

All photographs were analyzed by the author of the script. Due to the time required (approximately 1.2 hours) to analyze a complete data set of 36 measurements for a given temperature regime, it was not feasible to involve additional operators. As a result, a small bias may be present in the data presented in this report.

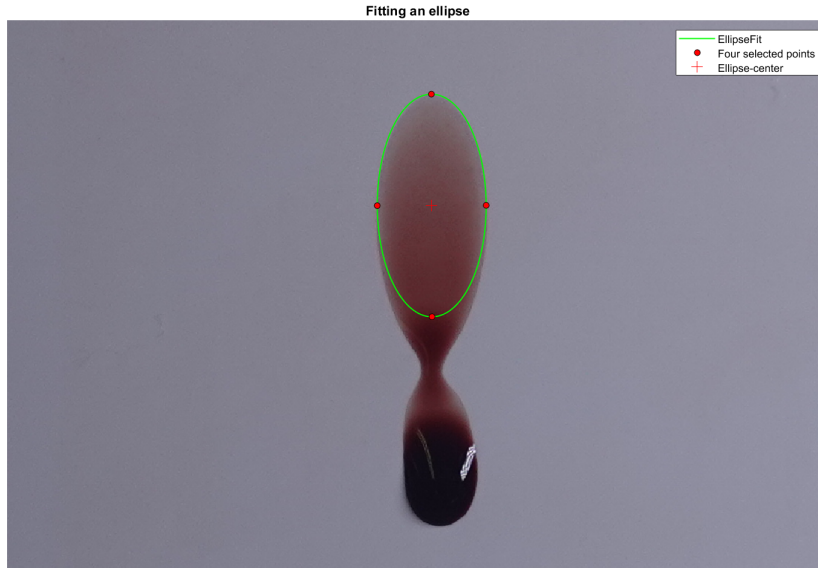


Figure 3.2: Ellipse fit of a bloodstain using our MATLAB script. The green outline represents the fitted ellipse, the red dots indicate the four points used for fitting, and the red cross marks the ellipses center. The stain shown was deposited on a ceramic surface at room temperature, photographed 45 seconds after impact, on a 60° inclined surface, from a drop height of 30 cm. The reference metric used in this figure is cut out for better illustration.

Initially, an alternative method was used to fit an ellipse, based on edge detection using MATLAB's Image Acquisition Toolbox and an ellipse fitting algorithm by Andrew et al. (1996)^[7] using the direct least squares method. However, during orienting test measurements, it became clear that this method would only work at room temperature and failed across the remaining boiling regimes. In the natural convection regime (around 90°C), the edges were too transparent to be detected due to blood separating into its components, while in the higher temperature regimes the bubbles generated by evaporation disturbed the interface, leading to inaccurate edge detection and thus unreliable measurements.

The blood droplet spreading will be presented using the general fluid spreading relation (Eq. 2.5), including blood droplets, found by Laan et al. (2015)^[14]:

$$\frac{W}{D_0} = \text{Re}^{1/5} \cdot \frac{P^{1/2} \sin \alpha}{(A + P^{1/2}(\sin \alpha)^{4/5})}$$

where the impact parameter $P = We Re^{-2/5}$ and $A = 1.24$ is a fitting parameter. The measured width W , the impact angle α , the initial droplet diameter D_0 , and the calculated impact velocity V_0 are then used for plotting Equation 2.5. The impact velocity can also be determined by numerically solving Equation 2.5. Numerically solving for the impact velocity was not performed in this research, because the calculated velocity values were not suitable for meaningful comparison.

Note that we do not measure the maximum width (W_{\max}) directly, but instead, we measure the width (W) a few seconds after impact. Due to capillary effects, the lamella retracts slightly, so the measured width and length are slightly smaller than the true maximum values. To accurately determine the maximum width and length, a high-speed camera positioned perpendicular to the surface could be used to analyze the spreading frame by frame and measure the ellipse width to find the maximum.

In practice, the initial droplet diameter cannot be determined directly by fitting an ellipse to the bloodstain. Laan et al. (2015)^[14] showed that it is possible to estimate the original volume of the blood droplet using 3D scanning of the surface. The initial droplet diameter can then be calculated by means of Equation 3.2.

3.5. Angle of impact and the W/L-ratio

Using the measured major axis as the length (L) and the minor axis as the width (W), the W/L-ratio as well as the angle of impact can be determined. Here, Equation 2.1 is used to calculate the impact angle:

$$\alpha = \arcsin\left(\frac{W}{L}\right)$$

which directly depends on the W/L-ratio.

With angles approaching 90° , it becomes clear that the measurement error in calculating the angle of impact increases dramatically. This is seen experimentally and can be shown mathematically (Equation 3.3 - 3.4).

Differentiating both sides of Equation 2.1 implicitly with respect to W/L gives:

$$\cos \alpha \cdot \frac{d(\alpha)}{d(W/L)} = 1 \quad (3.3)$$

rewriting,

$$d(\alpha) = \frac{1}{\cos \alpha} \cdot d(W/L). \quad (3.4)$$

When W/L approaches 1 (i.e., when the bloodstain becomes more circular), $1/\cos \alpha$ approaches infinity. This means that small deviations in the measured W/L -ratio lead to large uncertainties at high impact angles, as shown in Figure 3.3. Therefore, Equation 2.1 is considered inaccurate for impact angles in the range $75^\circ \leq \alpha \leq 90^\circ$, as indicated by the shaded gray area. Measurement errors of this type are mostly random, with the fitting measurements being performed by an experienced bloodstain analyst [13].

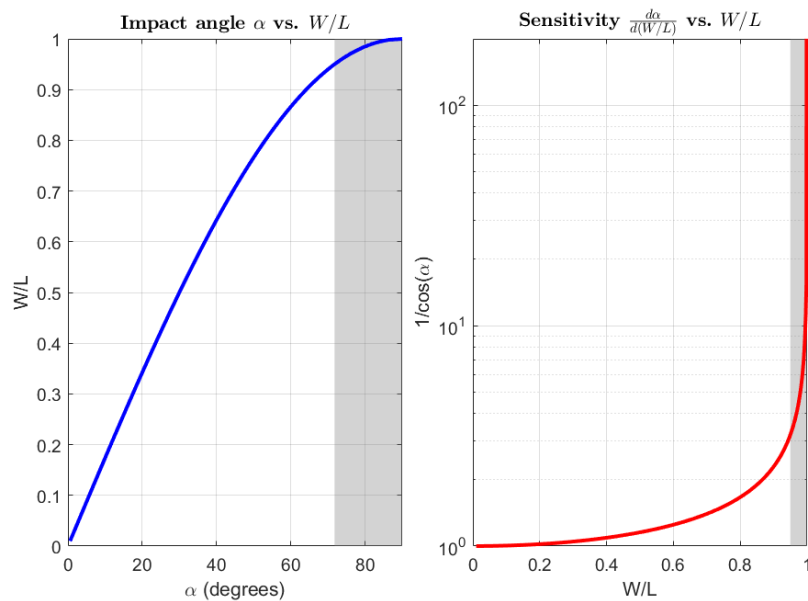


Figure 3.3: On the left, Equation 2.1 is plotted with the impact angle α (in degrees) on the x-axis and the W/L -ratio on the y-axis. On the right, the sensitivity function Equation 3.4 is shown. The shaded gray region ($75^\circ \leq \alpha \leq 90^\circ$) indicates the range in which Equation 2.1 becomes unreliable due to these amplified measurement errors.

In this research, experiments with an impact angle of 90° are still included. This choice was made to investigate potential significant deviations when measuring this angle on surfaces at different temperatures.

For largely inclined surfaces, it is observed that the blood continues to flow down along the surface after impact, elongating the ellipses length. The width generally does not change due to gravity, but the roughness of the surface and how much fluid it can absorb can alter both the width and length more. In the case of this research absorbency is not an issue. Therefore, the measurement error of the width is expected to be smaller than the error in the length. When fitting an ellipse manually (even automatically fitted ellipses have generally the same problem), the length is often overestimated, which results in a smaller predicted impact angle. A bloodstain with a well fitting ellipse and one with a poorly fitted (elongated) ellipse are shown in Figure 3.4.

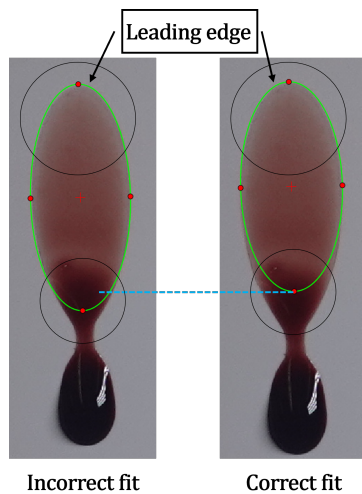


Figure 3.4: An ellipse fitted to the bloodstain resulting in an underestimation of the angle of impact (incorrect fit) and the ellipse that should be measured (correct fit). The differences in the ellipses include the length and how well they fit the bloodstain at the leading edge.

As an indication of accuracy, the mean deviation between the measured impact angle and the true angle is taken. And as an indication of precision, the mean standard deviation with a 95% confidence interval will be taken.

3.6. Data analysis

All data obtained from fitting an ellipse to a bloodstain, the self-made scripts used for ellipse fitting, and the further data analysis were performed in MATLAB R2023a. All plots presented in this report were also generated using these scripts. With the exception of the function that fits an ellipse given four corner points, the scripts are not included in this report due to their length. However, they have been a large part of the work done in this research and can be found in a GitHub repository at: <https://github.com/Mees-Bouwman/Blood-Heat-Project---Ellipse-Fitting-and-Data-Analysis-.git>

Measurement Indexing

To keep everything organized and make the data-analysis workflow easier, all measurements are organized using an indexing system, as shown in Table 3.4. When photographing the bloodstains, the corresponding parameter combination was written on a piece of paper and attached to the reference metric, like this $T_{i,j} I_j H_j$. Each photograph was then named using this parameter combination, which allows the data to be efficiently filtered and organized.

Table 3.4: Overview of Measurement Parameters and Indexing

Indexing		
Index	Description	Range
i	Repeats n	$i = 1$ to n , where $n = 3$
j	Variable number parameter k	$j = 1$ to k , where $k = \text{length}(\text{Parameter})$

Parameter Naming		
Parameter	Description	Values , k
$T_{i,j}$	Surface Temperature T_w [°C]	(90, 120, 160, 230), $k = 4$
I_j	Impact Angle α [°]	(90, 75, 60, 30), $k = 4$
H_j	Height h [cm]	(30, 60, 90), $k = 3$

Obtaining the Data

All photographs were analyzed using a self-written MATLAB script, the structure is illustrated in the flowchart below in Fig. 3.5. The resulting data, stored in a MATLAB table, were later filtered and visualized, which is easily done because of the used indexing system.

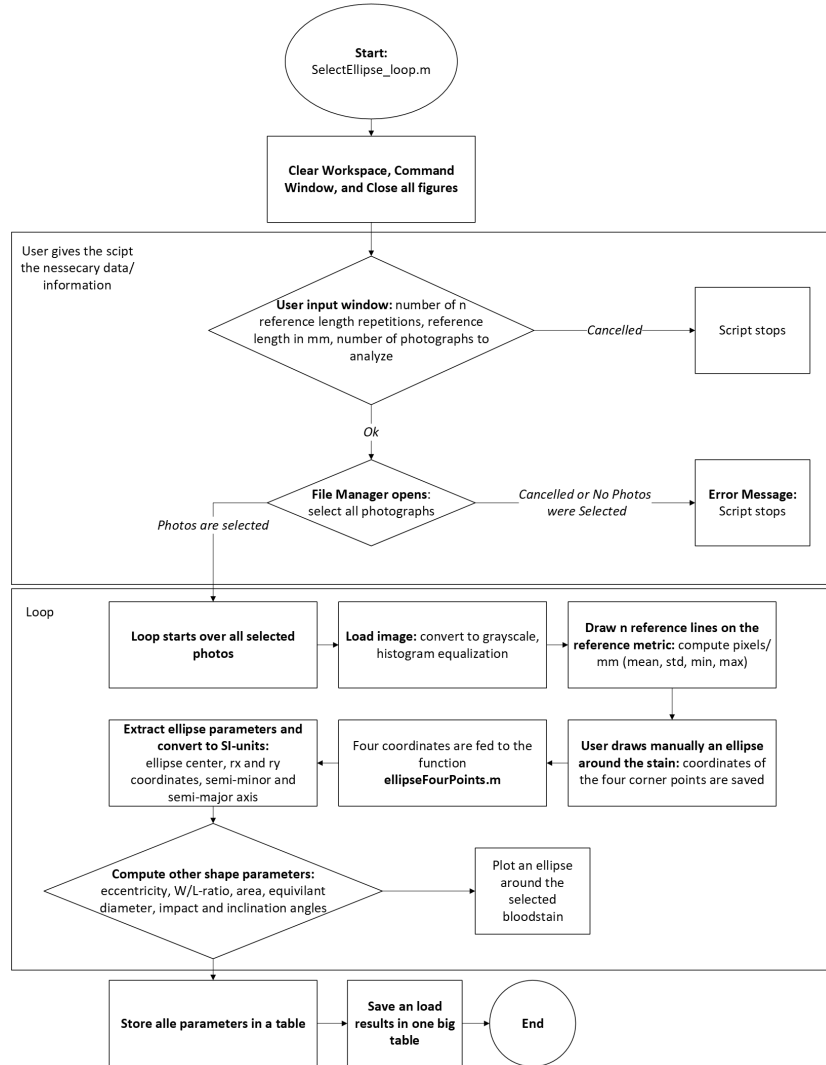


Figure 3.5: Flowchart of the MATLAB script used for bloodstain analysis. The diagram outlines the full workflow. The results are stored in a table.

Bloodstain Width Error, W

Ellipse measurements are expected to be random, with possibly a slight bias due to having only one operator. Parallax effects in the photographs can be considered negligible. The reference length calibration is accurate enough to disregard the uncertainty of ± 0.2 pixels per mm. The bloodstain width W is computed as the mean of three independent measurement repetitions. Therefore, the uncertainty is calculated using the Standard Error of the Mean, as shown in Equation 3.5:

$$\text{SEM}_{I,H} = \frac{SD_{I,H}}{\sqrt{N_{\text{repeats}}}} \quad (3.5)$$

where the indices I and H denote the index number of the impact angle and drop height, respectively. $N_{\text{repeats}} = 3$ represents the number of repetitions, and $SD_{I,H}$ is the standard deviation.

All measurements are assumed to be normally distributed. However, due to the small sample size of three, this assumption cannot be directly validated. To get a more accurate estimation of the errors, the two-sided Student's t-distribution is applied to $\text{SEM}_{I,H}$. The degrees of freedom are $df = 2$, and a confidence interval of $CI = 95\%$ ($\alpha = 0.05$) is used, resulting in a critical value of $t_{\text{crit}} \approx 4.303$.

Impact Angle Error, α

First it was checked if the impact velocity, in this research varied by the drop height, influenced the measurement or accuracy of the impact angle. As shown in Figure 3.6, the data points appear to be randomly scattered around the intended 'true' impact angle within the range of impact velocities used in this research, as the impact velocity increases this might not be true. But considering the small sample size, this conclusion may also be wrong. In Appendix C, the spread distribution of the remaining three angles are given. For simplicity, the impact angle is therefore averaged over the three heights.

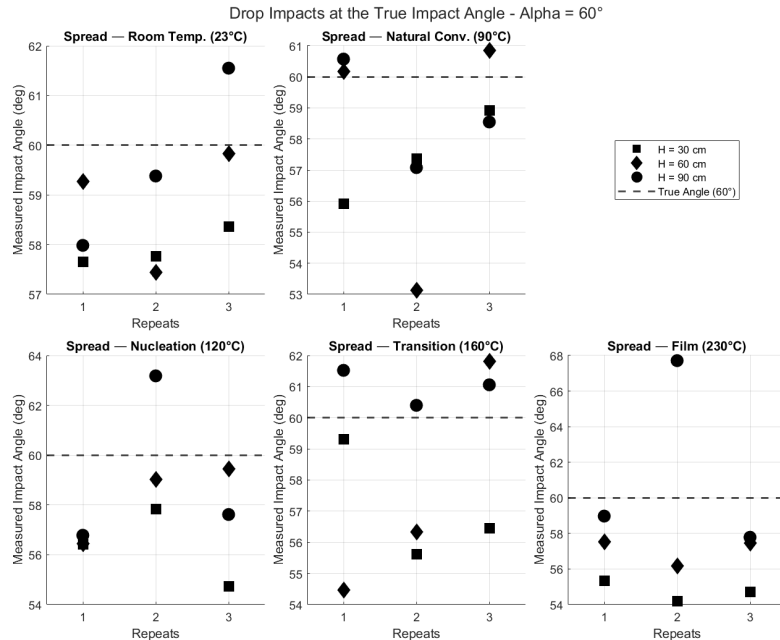


Figure 3.6: The spread of the measured impact angle at $\alpha = 60^\circ$ ($\theta = 30^\circ$) with three different drop heights. Each data point is an average of 3 blood drops ($N = 3$). It seems that the drop height (i.e. the impact velocity) does not affect the accuracy of the impact angle.

Accuracy. The accuracy of the impact angle is defined as the absolute difference between the average measured impact angle $\bar{\alpha}$ and the true impact angle α_{true} , as given in Equation 3.6.

$$\delta_{I,H} = |\bar{\alpha}(I,H) - \alpha_{\text{true}}| \quad (3.6)$$

Precision. As an indication of the precision of the measured impact angle α , the aggregated Standard Error of the Mean ($SEM_{\text{over}H}$) was calculated. Since the impact angle was averaged over multiple drop heights, the combined variance is obtained by taking a linear combination of the individual variances $\text{Var}(\bar{\alpha}_{I,H_i})$, each weighted by a constant $c_i = (1/N_H)^2$:

$$\text{Var}(\bar{\alpha}_{I, \text{over}H}) = \sum_{i=1}^{N_H} \left(\frac{1}{N_H} \right)^2 \text{Var}(\bar{\alpha}_{I,H_i}) \quad (3.7)$$

The Standard Error of the Mean (SEM) is defined as the square root of the variance. Because the impact angle was averaged over three drop heights, $N_H = 3$. Therefore,

$$SEM_{\bar{\alpha}_{I, \text{over}H}} = \sqrt{\frac{1}{3^2} \sum_{i=1}^3 SEM_{I,H_i}^2} = \frac{1}{3} \sqrt{\sum_{i=1}^3 SEM_{I,H_i}^2}. \quad (3.8)$$

For the same reason as for the bloodstain width, the error of the impact angle is multiplied by the critical value $t_{\text{crit}} \approx 4.303$ from the Student's t-distribution.

4

Results and Interpretation

4.1. Effect of Temperature and Impact Angle Upon the Bloodstain Width, W

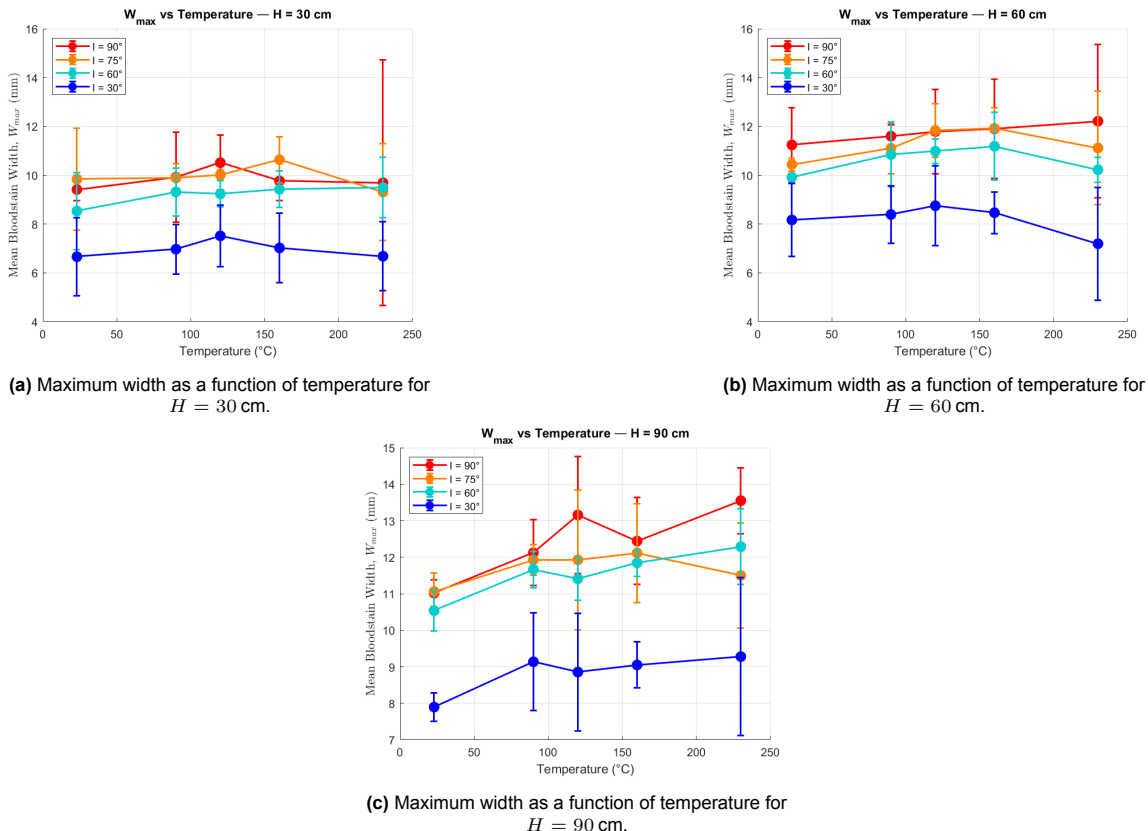


Figure 4.1: Maximum width (W_{\max}) as a function of temperature for three different heights (H).

4.2. Blood impacts in different boiling regimes

Blood impacts in room temperature

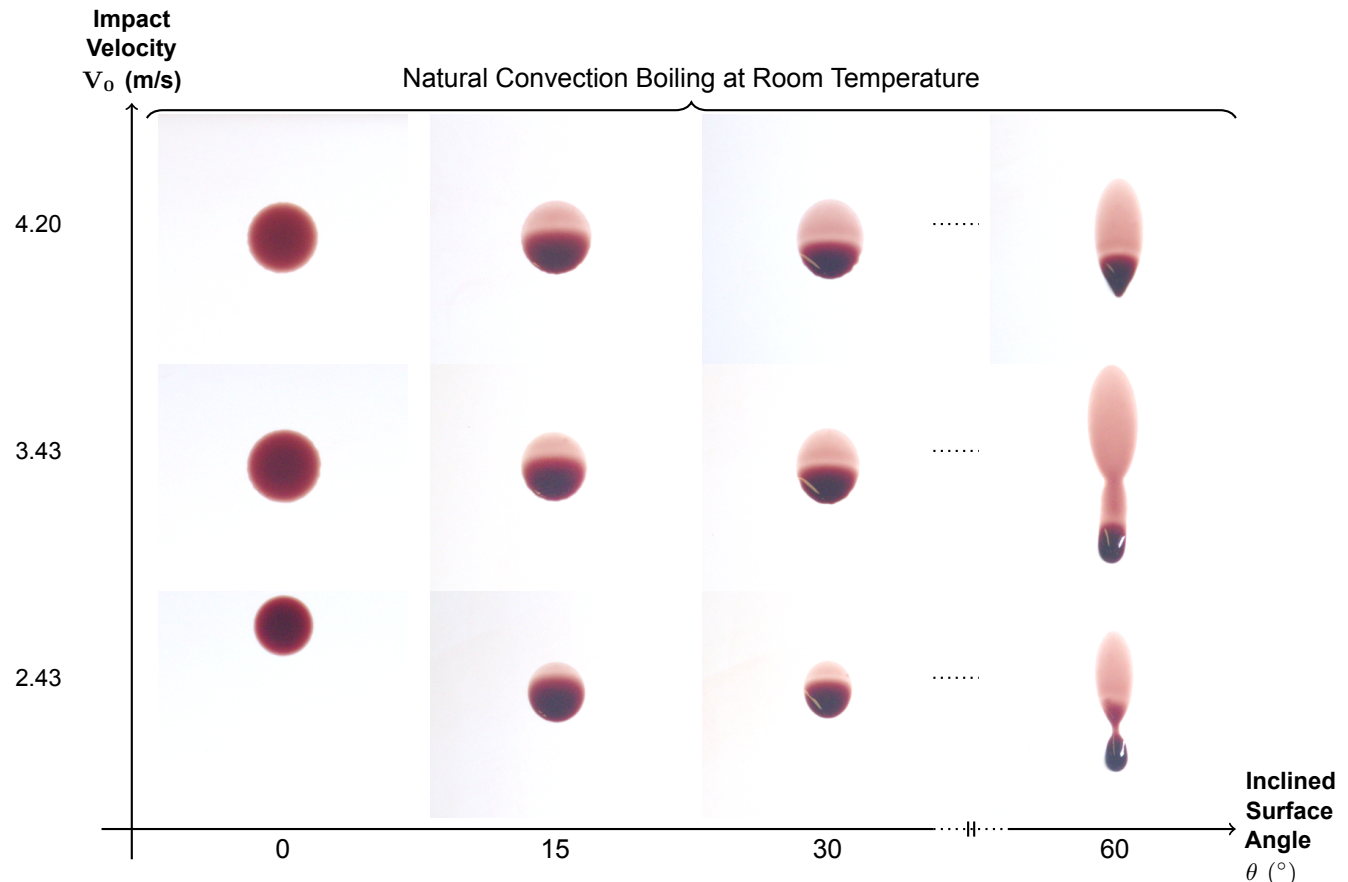


Figure 4.2: Recorded pictures 45 seconds after impact of the passive drip stains on a specific surface temperature. In this figure the surface was at room temperature $\sim 23^{\circ}C$ (Repeat 2). Deformation of the stain increases with velocity (bottom to top) and with surface inclination (left to right).

Blood impacts in the Natural Convection Regime

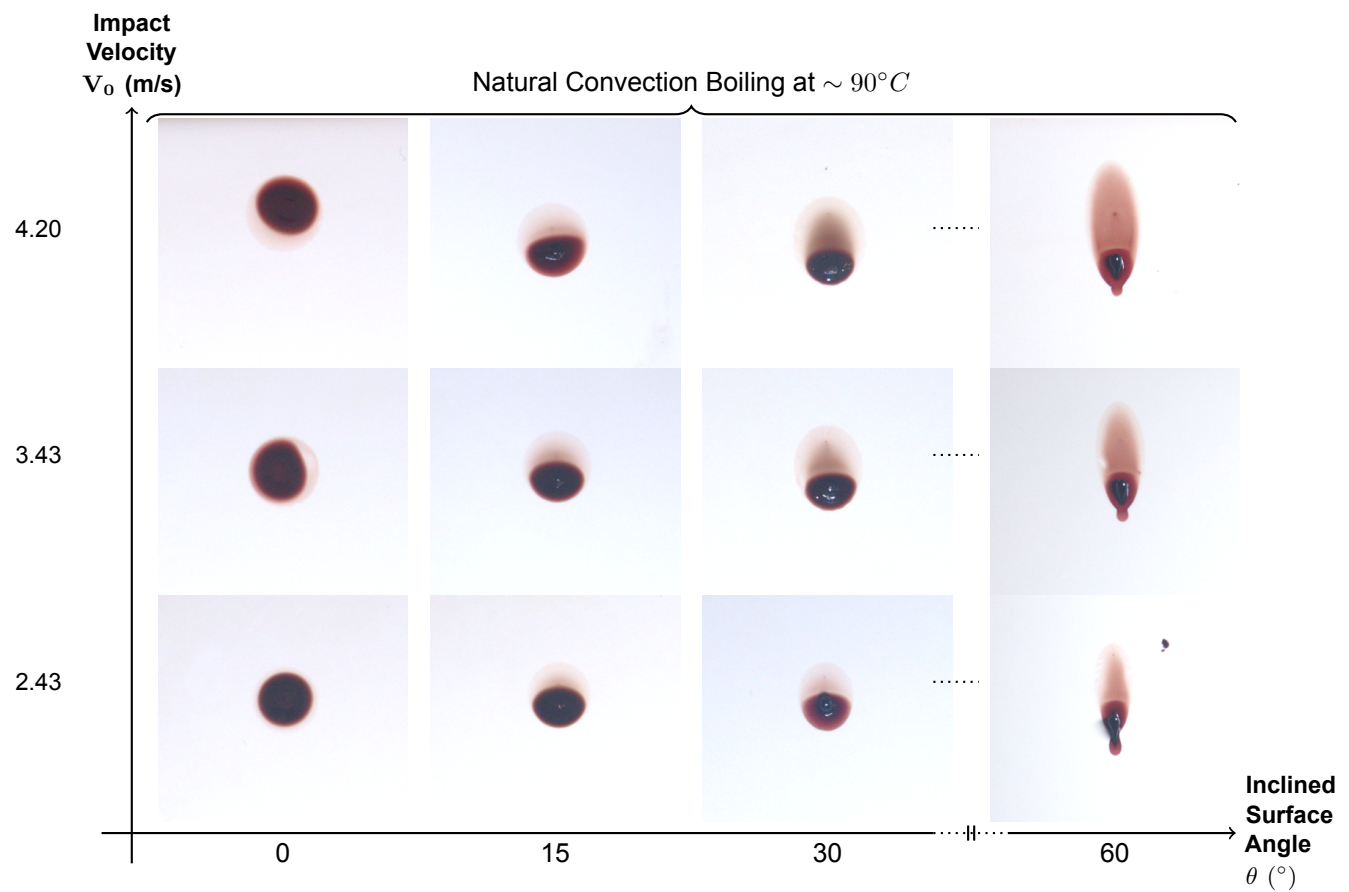


Figure 4.3: Recorded pictures 45 seconds after impact of the passive drip stains on a specific surface temperature. In this figure the surface was heated to a temperature of $\sim 90^{\circ}\text{C}$ (Repeat 2). Deformation of the stain increases with velocity (bottom to top) and with surface inclination (left to right).

Blood Impacts in the Nucleation-Boiling Regime

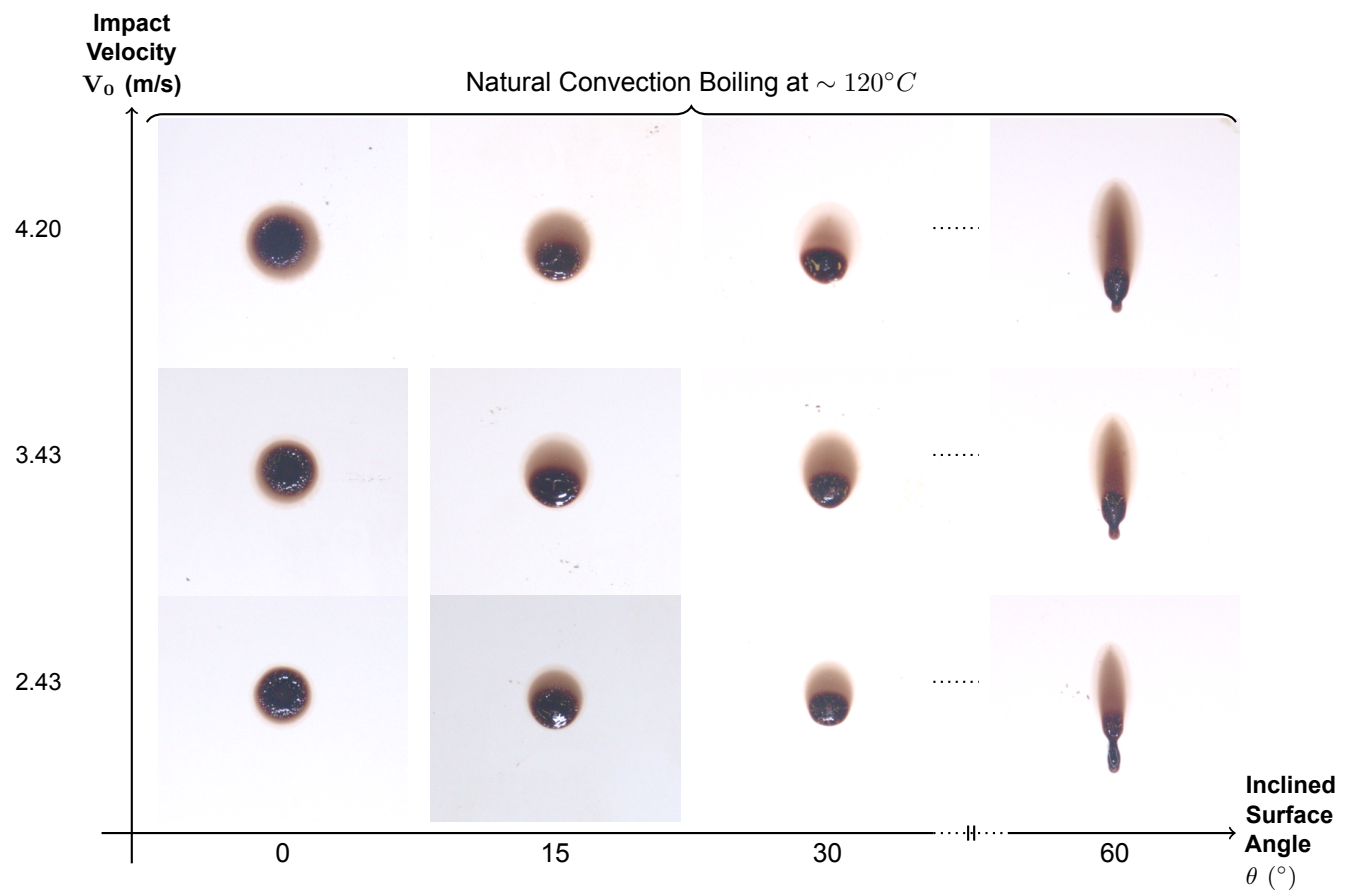


Figure 4.4: Recorded pictures 45 seconds after impact of the passive drip stains on a specific surface temperature. In this figure the surface was heated to a temperature of $\sim 120^\circ C$ (Repeat 2). Deformation of the stain increases with velocity (bottom to top) and with surface inclination (left to right).

Blood Impacts in the Transition-Boiling Regime

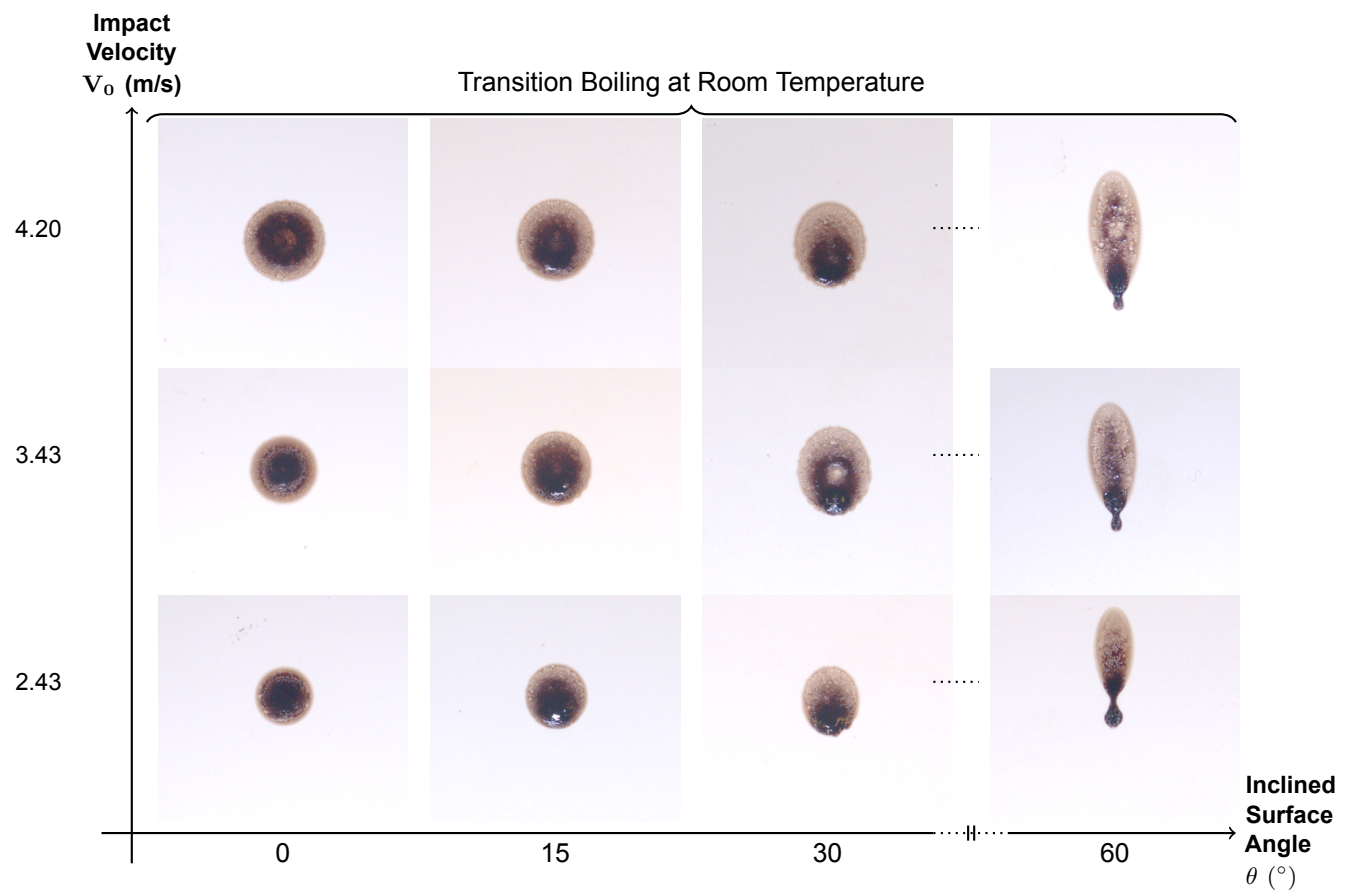


Figure 4.5: Recorded pictures 45 seconds after impact of the passive drip stains on a specific surface temperature. In this figure the surface was heated to a temperature of $\sim 160^\circ\text{C}$ (Repeat 1). Deformation of the stain increases with velocity (bottom to top) and with surface inclination (left to right).

Blood Impacts in the Film Boiling Regime

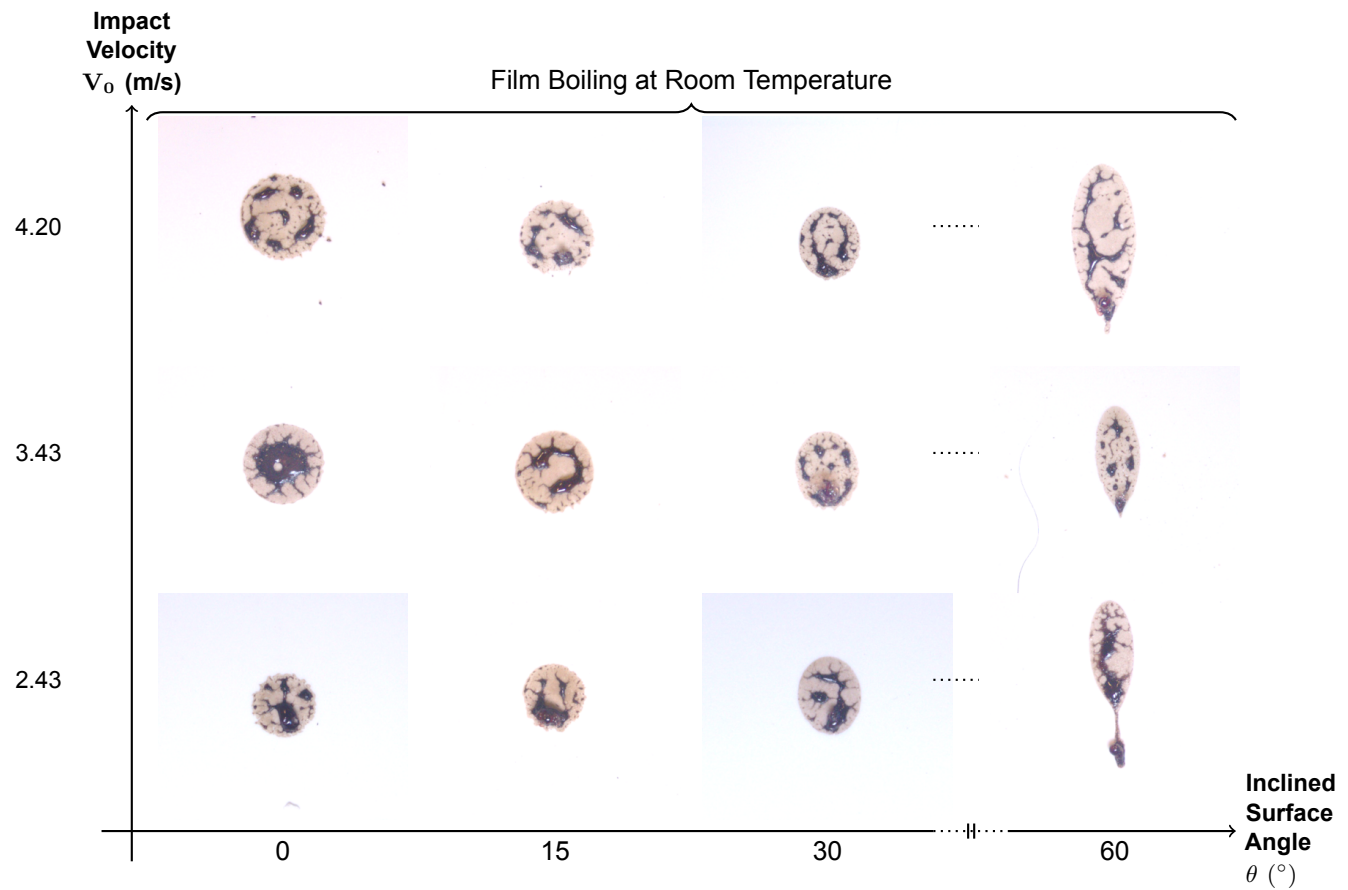


Figure 4.6: Recorded pictures 45 seconds after impact of the passive drip stains on a specific surface temperature. In this figure the surface was heated to a temperature of $\sim 230^\circ\text{C}$ (Repeat 2). Deformation of the stain increases with velocity (bottom to top) and with surface inclination (left to right).

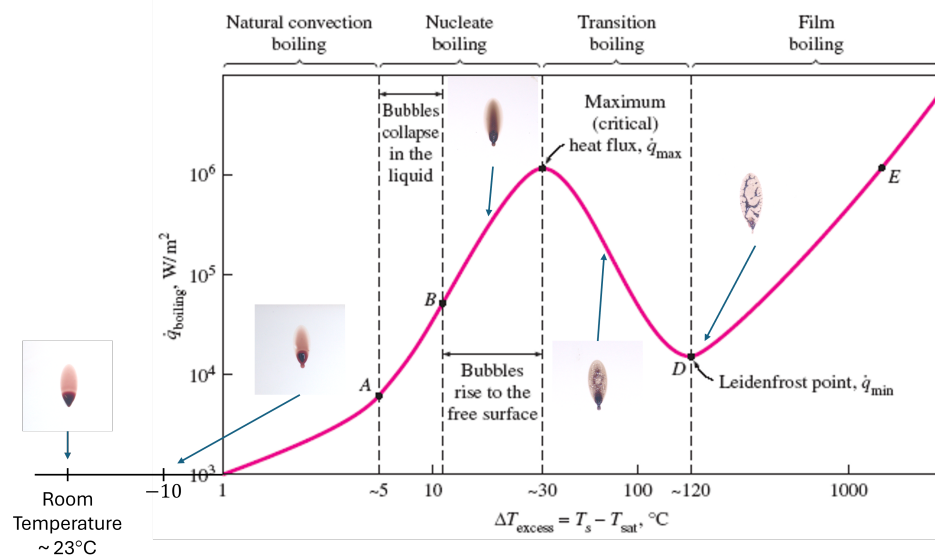


Figure 4.7: Summary of blood droplet impact behavior on a heated surface shown within the classical boiling-curve regime of water. The images illustrate stain patterns of droplets impacting at a 30° angle from a drop height of 90 cm. As the surface temperature increases, the droplet morphology

4.3. Impact angle

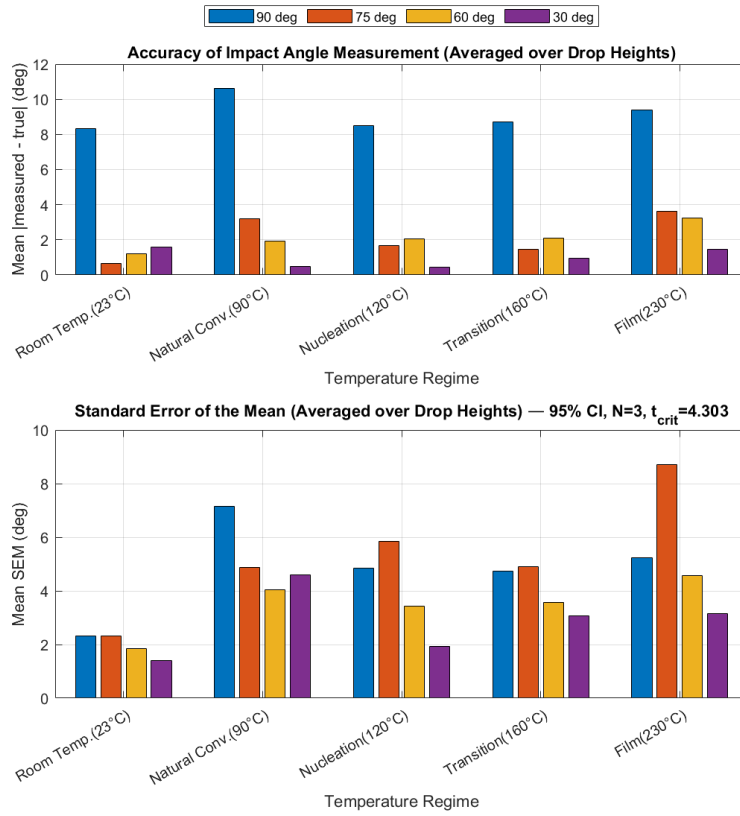


Figure 4.8: Caption

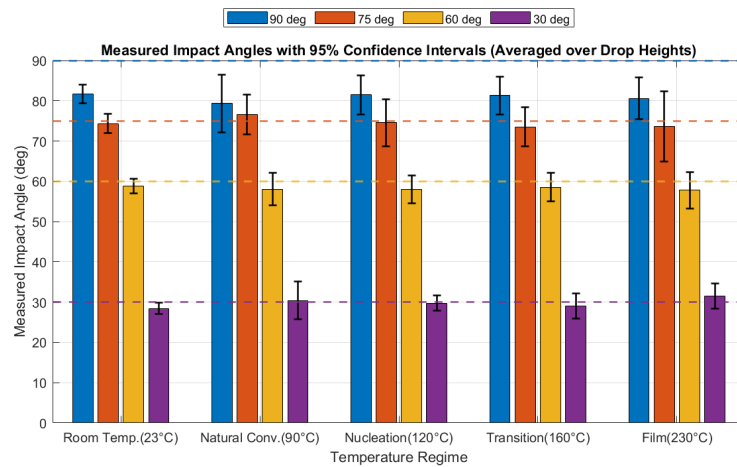


Figure 4.9: Caption

4.4. Droplet spreading

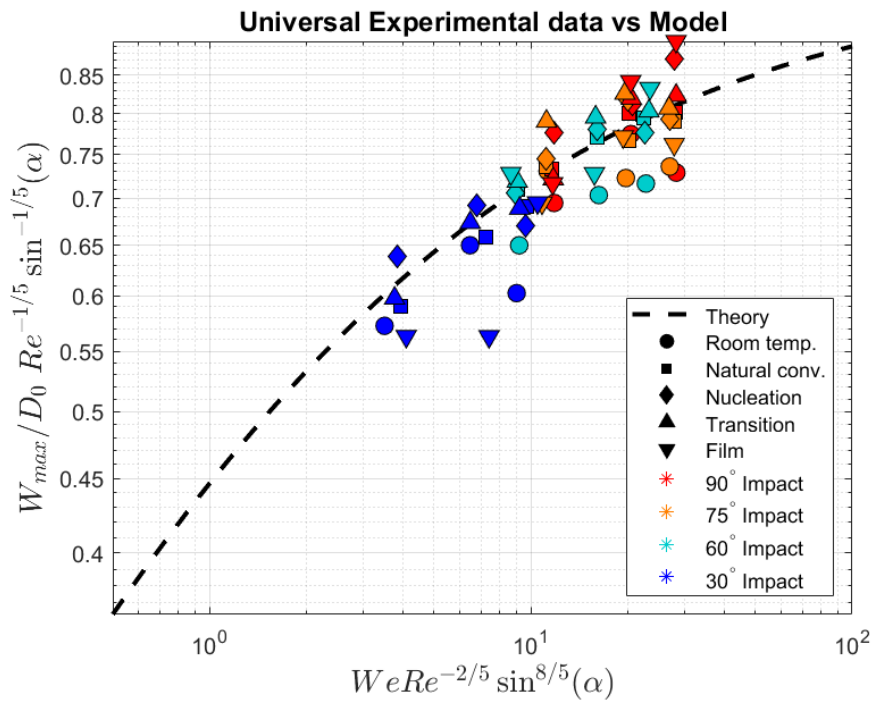


Figure 4.10: Caption

5

Development New Experimental Setup

6

Discussion

A discussion

7

Conclusion

A conclusion...

8

Recommendations and Outlook

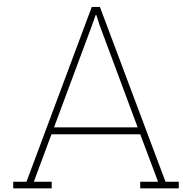
Some recommendations and an outlook from our perspective for the future of this research.

References

- [1] V. Balthazard et al. "Étude des gouttes de sang projeté". In: *Annales de Médecine Légale de Criminologie, Police Scientifique, Médecine Sociale et Toxicologie* 19 (1939), pp. 265–323.
- [2] W. Barmore, T. Bajwa, and B. Burns. *Biochemistry, Clotting Factors*. 2023. URL: <https://www.ncbi.nlm.nih.gov/books/NBK507850/>.
- [3] Belinda Bastide, Glenn Porter, and Adrian Renshaw. "The effects of heat on the physical and spectral properties of bloodstains at arson scenes". In: *Forensic Science International* 325 (2021), p. 110891. ISSN: 0379-0738. DOI: <https://doi.org/10.1016/j.forsciint.2021.110891>. URL: <https://www.sciencedirect.com/science/article/pii/S0379073821002115>.
- [4] David Brutin et al. "Patterns Formation in Drying Drops of Blood". In: *Journal of Fluid Mechanics* 667 (Jan. 2011), pp. 85–95. DOI: [10.1017/S0022112010005070](https://doi.org/10.1017/S0022112010005070).
- [5] R. Chaudhry, R.B. Killeen, and H.M. Babiker. *Physiology, Coagulation Pathways*. 2025. URL: <https://www.ncbi.nlm.nih.gov/books/NBK482253/>.
- [6] Farlex. *Defibrinated blood*. <https://medical-dictionary.thefreedictionary.com/defibrinated+blood>. Accessed: 2025-12-09.
- [7] Andrew Fitzgibbon, M. Pilu, and Robert Fisher. "Direct Least-squares fitting of ellipses". In: vol. 21. Sept. 1996, 253–257 vol.1. ISBN: 0-8186-7282-X. DOI: [10.1109/ICPR.1996.546029](https://doi.org/10.1109/ICPR.1996.546029).
- [8] V.Suneetha G.Shibu. "Medium-Velocity Impact Blood Spatter Analysis". In: *International Journal of Drug Development and Research* (2015).
- [9] {Marise Vera} Gielen. "Splashing Drops". English. PhD Thesis - Research external, graduation UT. University of Twente, 2018. ISBN: 978-90-365-4495-5. DOI: [10.3990/1.9789036544955](https://doi.org/10.3990/1.9789036544955).
- [10] K. J. Gregg and M. K. Brown. "Blood Pattern Analysis: The Morphology of Blood Drops on Heated Surfaces". Onuitgegeven manuscript, School of Science, Engineering & Design, Teesside University. n.d.
- [11] Ryuta Hatakenaka and Yoshiyuki Tagawa. "Drop impact onto a heated surface in a depressurized environment". In: *International Journal of Heat and Mass Transfer* 247 (2025), p. 126959. ISSN: 0017-9310. DOI: <https://doi.org/10.1016/j.ijheatmasstransfer.2025.126959>. URL: <https://www.sciencedirect.com/science/article/pii/S001793102500300X>.
- [12] L. Hulse-Smith, N. Z. Mehdizadeh, and S. Chandra. "Deducing drop size and impact velocity from circular bloodstains". In: *Journal of Forensic Sciences* 50.1 (2005), pp. 54–63.
- [13] Joanna Kathleen. *Investigation of factors affecting the region of origin estimate in bloodstain pattern analysis*. UC Research Repository, University of Canterbury. 2006. DOI: <http://dx.doi.org/10.26021/9025>.
- [14] N. Laan. "Impact of blood droplets". PhD thesis, Van der Waals-Zeeman Institute, FNWI. PhD thesis. Universiteit van Amsterdam, Nov. 2015. ISBN: 9789462598751. URL: <https://dare.uva.nl/search?identifier=ec9bf9ce-21c1-4e3a-9435-7a623286da4b>.
- [15] Nick Laan et al. "Morphology of drying blood pools". In: *Forensic Science International* 267 (2016), pp. 104–109. ISSN: 0379-0738. DOI: <https://doi.org/10.1016/j.forsciint.2016.08.005>. URL: <https://www.sciencedirect.com/science/article/pii/S0379073816303358>.
- [16] Bethany A. J. Larkin and Craig E. Banks. "Preliminary study on the effect of heated surfaces upon bloodstain pattern analysis". In: *Journal of Forensic Sciences* 58.5 (2013), pp. 1289–1296. DOI: [10.1111/1556-4029.12185](https://doi.org/10.1111/1556-4029.12185).
- [17] L. Barksdale M.Benecke. "Distinction of bloodstain patterns from fly artifacts". In: *Forensic Science International* (2003). DOI: [10.1016/j.forsciint.2003.07.012](https://doi.org/10.1016/j.forsciint.2003.07.012).

- [18] Marco Marengo et al. "Drop collisions with simple and complex surfaces". In: *Current Opinion in Colloid & Interface Science* 16.4 (2011), pp. 292–302. ISSN: 1359-0294. DOI: <https://doi.org/10.1016/j.cocis.2011.06.009>. URL: <https://www.sciencedirect.com/science/article/pii/S1359029411000859>.
- [19] Elaine N. Marieb and Katja Hoehn. *Human Anatomy & Physiology*. 7th ed. San Francisco: Pearson Benjamin Cummings, 2010, pp. 648–650.
- [20] H. Marmanis and S. T. Thoroddsen. "Scaling of the fingering pattern of an impacting drop". In: *Physics of Fluids* 8.6 (June 1996), pp. 1344–1346. ISSN: 1070-6631. DOI: <10.1063/1.868941>. eprint: https://pubs.aip.org/aip/pof/article-pdf/8/6/1344/19050076/1344_1_online.pdf. URL: <https://doi.org/10.1063/1.868941>.
- [21] NAVID MEHDIZADEH and SANJEEV CHANDRA. "Formation of fingers around the edge of a drop hitting a metal plate". In: *Journal of Fluid Mechanics* 510 (July 2004), pp. 353–373. DOI: <10.1017/S0022112004009310>.
- [22] Elie Nader et al. "Blood Rheology: Key Parameters, Impact on Blood Flow, Role in Sickle Cell Disease and Effects of Exercise". In: *Frontiers in Physiology* Volume 10 - 2019 (2019). ISSN: 1664-042X. DOI: <10.3389/fphys.2019.01329>. URL: <https://www.frontiersin.org/journals/physiology/articles/10.3389/fphys.2019.01329>.
- [23] V.E. Nakoryakov, S.Ya. Misyura, and S.L. Elistratov. "The behavior of water droplets on the heated surface". In: *International Journal of Heat and Mass Transfer* 55.23 (2012), pp. 6609–6617. ISSN: 0017-9310. DOI: <https://doi.org/10.1016/j.ijheatmasstransfer.2012.06.069>. URL: <https://www.sciencedirect.com/science/article/pii/S0017931012005005>.
- [24] Lucy A Norris. "Blood coagulation". In: *Best Practice & Research Clinical Obstetrics & Gynaecology* 17.3 (2003). Inherited Thrombophilias, pp. 369–383. ISSN: 1521-6934. DOI: [https://doi.org/10.1016/S1521-6934\(03\)00014-2](https://doi.org/10.1016/S1521-6934(03)00014-2). URL: <https://www.sciencedirect.com/science/article/pii/S1521693403000142>.
- [25] Ali Ostadfar. "Chapter 1 - Fluid Mechanics and Biofluids Principles". In: *Biofluid Mechanics*. Ed. by Ali Ostadfar. Academic Press, 2016, pp. 1–60. ISBN: 978-0-12-802408-9. DOI: <https://doi.org/10.1016/B978-0-12-802408-9.00001-6>. URL: <https://www.sciencedirect.com/science/article/pii/B9780128024089000016>.
- [26] Sidney Perkowitz. *The physics of blood spatter*. Oct. 17, 2019. URL: <https://physicsworld.com/a/the-physics-of-blood-spatter/> (visited on 11/20/2025).
- [27] J.Wu R.Baby S.Michielsen. "Effects of yarn size and blood drop size on wicking and bloodstains in textiles". In: (Mar. 2021). DOI: <10.1111/1556-4029.14702>. URL: <https://onlinelibrary.wiley.com/doi/10.1111/1556-4029.14702>.
- [28] Ilia Roisman, Romain Rioboo, and Cameron Tropea. "Normal impact of a liquid drop on a dry surface: Model for spreading and receding". In: *Proceedings of The Royal Society A: Mathematical, Physical and Engineering Sciences* 458 (June 2002), pp. 1411–1430. DOI: <10.1098/rspa.2001.0923>.
- [29] T.P. SUtto S.H. James P.E. Kish. *Principles of Bloodstain Pattern Analysis*. Taylor & Francis, 2005.
- [30] J.C.Bird S.Shiri K.F.Martin. "Surface coatings including fingerprint residues can significantly alter the size and shape of bloodstains". In: (Feb. 2019), pp. 189–198. DOI: <10.1016/j.forsciint.2018.12.008>. URL: <https://www.sciencedirect.com/science/article/pii/S0379073818310600>.
- [31] R. K. Singh et al. "Evaporation of water droplets impacting upon heated surfaces". In: *The International Journal of Engineering and Science (IJES)* 2020 (2020), pp. 61–67.
- [32] P. D. Sturkie and P. Griminger. "Blood: Physical Characteristics, Formed Elements, Hemoglobin, and Coagulation". In: *Avian Physiology*. Ed. by P. D. Sturkie. Berlin, Heidelberg: Springer Berlin Heidelberg, 1976, pp. 53–75. ISBN: 978-3-642-96274-5. DOI: 10.1007/978-3-642-96274-5_3. URL: https://doi.org/10.1007/978-3-642-96274-5_3.
- [33] user948761. *Approximating an Ellipse given 4 points*. (version: 2022-06-14). URL: <https://math.stackexchange.com/q/4471344>.

- [34] Autilia Vitiello et al. "Bloodstain pattern analysis as optimisation problem." In: *Forensic science international* 266 (2016). URL: <https://api.semanticscholar.org/CorpusID:3472753>.
- [35] Adam Wesolowski and Anna Mlynarczak. "Surface Tension and Viscosity of Blood". In: (July 2019). DOI: [10.20944/preprints201907.0090.v1](https://doi.org/10.20944/preprints201907.0090.v1).
- [36] Siddharth Singh Yadav et al. "Surface tension measurement of normal human blood samples by pendant drop method". In: *Journal of Medical Engineering & Technology* 44.5 (2020). PMID: 32589070, pp. 227–236. DOI: [10.1080/03091902.2020.1770348](https://doi.org/10.1080/03091902.2020.1770348). eprint: <https://doi.org/10.1080/03091902.2020.1770348>. URL: <https://doi.org/10.1080/03091902.2020.1770348>.
- [37] Guangya Zhu et al. "Evaporation characteristics of water droplets on heated surfaces with various coatings and under different wall thermal conditions". In: *Experimental Thermal and Fluid Science* 160 (2025), p. 111335. ISSN: 0894-1777. DOI: <https://doi.org/10.1016/j.expthermflusci.2024.111335>. URL: <https://www.sciencedirect.com/science/article/pii/S0894177724002048>.



Derivation of the Impact Velocity Using Bernoulli's Law

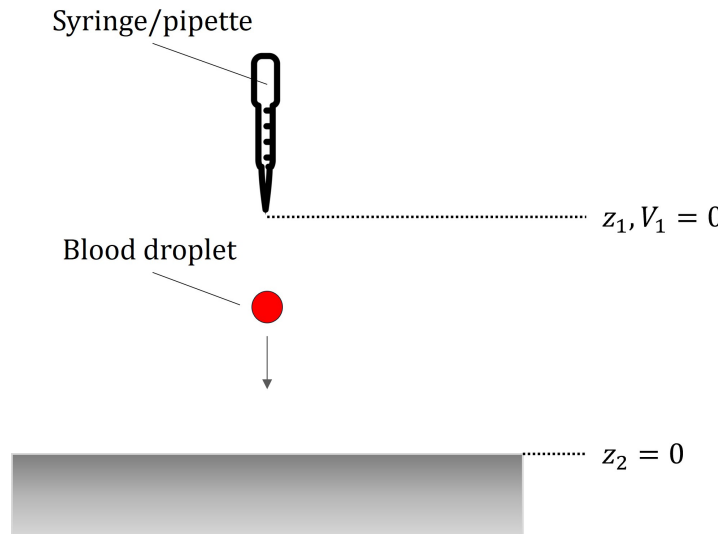


Figure A.1: Schematic of the drop impact situation.

Bernoulli's equation states:

$$P_1 + \frac{1}{2}\rho V_1^2 + \rho g z_1 = P_2 + \frac{1}{2}\rho V_2^2 + \rho g z_2 \quad (\text{A.1})$$

Assume the following conditions:

$$\begin{cases} P_1 = P_2 = P & \text{(pressure is equal at both points)} \\ V_1 = 0 & \text{(initial velocity is negligible)} \\ z_2 = 0 & \text{(reference level at point 2)} \end{cases}$$

Substituting these into Bernoulli's equation gives:

$$\rho g z_1 = \frac{1}{2}\rho V_2^2 \quad (\text{A.2})$$

Dividing both sides by ρ :

$$gz_1 = \frac{1}{2}V_2^2 \quad (\text{A.3})$$

Solving for V_2 gives:

$$V_2 = \sqrt{2gz_1} \quad (\text{A.4})$$

If we denote the drop height as h , this can be written as:

$$\boxed{V_0(h) = \sqrt{2gh}} \quad (\text{A.5})$$

B

Approximating an Ellipse given 4 corner points + MATLAB code translation

The mathematical derivation used for approximating an ellipse given 4 points is by user948761 from Mathematics Stack Exchange [33].

All self-made MATLAB scripts can be found in a GitHub repository at: <https://github.com/Mees-Bouwman/Blood-Heat-Project---Ellipse-Fitting-and-Data-Analysis-.git>.

```
% Function that fits an ellipse using four known coordinates
% Name: Mees Bouwman
% Date: 19-10-2025
% Study program: Applied Physics
% Year: 3
% Assignment/Project: Smart Solutions Semester (3S) – Blood & Heat

% The mathematical derivation used for fitting an ellipse
% through four given points is described in the following math forum:
% https://math.stackexchange.com/questions/4471307/approximating-an-ellipse-given-4-points

% This function uses another function that calculates the area
% of the drawn ellipse, called '[Opp] = ellipsoppvervlak(a)'.
% This is the second function (sub-function) within this script.

function [r0, rx, ry, semi_major, semi_minor] = ellipseFourPoints(P1, P2, P3, P4)

% r0 = 'center of ellipse' a 2x1 vector
% rx and ry are the coordinates for plotting the ellipse, an array
% semi_major = 'half the of longest length', a scalar (float)
% semi_minor = 'half the of shortest length', a scalar (float)
% P1 to P4 are the four points/coordinates where a ellipse is fitted to,
% these are an 1x2 vector. P(1) is the x-component and P(2) is the
% y-component.
```

You have 4 points $P_k = (x_k, y_k)$, $k = 1, 2, 3, 4$. And you want to generate the equation of an ellipse that passes through these four points. Such an ellipse would have to satisfy the general conic equation:

$$Ax^2 + Bxy + Cy^2 + Dx + Ey + F = 0 \quad (\text{B.1})$$

For an ellipse A cannot be zero, thus for each of the four points, the equation becomes

```
% In the code A is set equal to 1
```

$$x_k^2 + Bx_ky_k + Cy_k^2 + Dx_k + Ey_k + F = 0, \quad k = 1, 2, 3, 4 \quad (\text{B.2})$$

And this is a 4×5 linear system in the five unknowns B, C, D, E, F ,

$$Qa = b \quad (\text{B.3})$$

where

$$Q = \begin{bmatrix} x_1y_1 & y_1^2 & x_1 & y_1 & 1 \\ x_2y_2 & y_2^2 & x_2 & y_2 & 1 \\ x_3y_3 & y_3^2 & x_3 & y_3 & 1 \\ x_4y_4 & y_4^2 & x_4 & y_4 & 1 \end{bmatrix}$$

$$\begin{aligned} Q = [P1(1)*P1(2), P1(2)^2, P1(1), P1(2), 1; \\ P2(1)*P2(2), P2(2)^2, P2(1), P2(2), 1; \\ P3(1)*P3(2), P3(2)^2, P3(1), P3(2), 1; \\ P4(1)*P4(2), P4(2)^2, P4(1), P4(2), 1]; \end{aligned}$$

$$a = [B, C, D, E, F]^T$$

$$b = [-x_1^2, -x_2^2, -x_3^2, -x_4^2]^T$$

$$b = \text{transpose}([-P1(1)^2, -P2(1)^2, -P3(1)^2, -P4(1)^2]);$$

Assuming Q has full row rank (i.e., assuming it has 4 linearly independent rows), then, we can write

$$a = Q^T u + w \quad (\text{B.4})$$

where w is in the null space of Q , and $u \in \mathbb{R}^4$. It follows that

$$w = \text{null}(Q); \quad \% \text{ null()} \text{ returns an orthonormal basis (unit lenght) for the null space of } A$$

$$Q(Q^T u + w) = b \quad (\text{B.5})$$

which reduces to

$$QQ^T u = b \quad (\text{B.6})$$

Therefore,

$$u = (QQ^T)^{-1}b \quad (\text{B.7})$$

$$u = (Q * Q') \setminus b; \quad \% \setminus \text{ is an inverse operator for matrices, the matrice before the } \setminus \text{ sign is taken an inverse of, and ' is equal to transpose() }$$

And

$$a = Q^T u + w = V + tW \quad (*) \quad (\text{B.8})$$

where

$$V = Q^T(QQ^T)^{-1}b, \quad (\text{B.9})$$

or just

$$V = Q^T u, \quad (\text{B.10})$$

```
V = Q' * u;
```

and W is a fixed vector in the one-dimensional null space of Q .

```
W = w / norm(w); % norm() returns the magnitude of a vector, a scalar
```

To ensure that we get an ellipse, we have to impose the condition:

$$C - \frac{1}{4}B^2 > 0 \quad (\text{B.11})$$

So that

$$(V_2 + tW_2) - \frac{1}{4}(V_1 + tW_1)^2 > 0 \quad (\text{B.12})$$

And this re-arranges to

$$W_1^2 t^2 + (2V_1 W_1 - 4W_2)t + (V_1^2 - 4V_2) < 0 \quad (\text{B.13})$$

And the solution of this inequality is the interval $[t_1, t_2]$ where t_1, t_2 are the two roots of the quadratic on the left, $t_1 < t_2$.

```
W1 = W(1); W2 = W(2); V1 = V(1); V2 = V(2);
poly_coeffi = [W1^2, (2 * V1 * W1 - 4 * W2), (V1^2 - 4 * V2)];
roots_poly_coeffi = roots(poly_coeffi);

% t1 < t2
t1 = min(roots_poly_coeffi);
t2 = max(roots_poly_coeffi);

% t in [t1 t2] represents the range of values where a valid ellipse exists
% t_optimal is the value that corresponds to the ellipse with the minimum area
% This is determined using the function ellipsoppvervlak. The whole function is given
% below.

Opp_function = @(t) ellipsoppvervlak(V + t * W);
t_optimaal = fminbnd(Opp_function, t1, t2);
a = transpose(V + t_optimaal * W);
```

Finally, once you select $t \in [t_1, t_2]$ and obtain a , then you have the ellipse equation in algebraic form

$$x^2 + Bxy + Cy^2 + Dx + Ey + F = 0 \quad (\text{B.14})$$

```
A = 1; B = a(1); C = a(2); D = a(3); E = a(4); F = a(5);
```

To draw this ellipse, you need to find the vector equation of the ellipse, i.e., you want to express the points (x, y) in terms of the center and semi-minor and semi-major axes vectors.

Define

$$r = [x, y]^T \quad (\text{B.15})$$

$$Q = \begin{bmatrix} 1 & \frac{B}{2} \\ \frac{B}{2} & C \end{bmatrix} \quad (\text{B.16})$$

```
q = [A, B/2;
      B/2, C];
```

This is a new Q not to be confused with the Q described in the previous analysis.

Also, define the vector

$$G = \begin{bmatrix} D \\ E \end{bmatrix} \quad (\text{B.17})$$

$$G = [D; E];$$

Now the algebraic equation of the ellipse is

$$r^T Q r + r^T G + F = 0 \quad (\text{B.18})$$

Start by finding the center of the ellipse. It is given by

$$r_0 = -\frac{1}{2}Q^{-1}G \quad (\text{B.19})$$

$$r0 = -0.5 * (q \setminus G); \quad \% \text{ center ellips}$$

Substituting this, the above algebraic equation of the ellipse becomes

$$(r - r_0)^T Q(r - r_0) = r_0^T Q r_0 - F \quad (\text{B.20})$$

Dividing through by the right hand side, yields

$$(r - r_0)^T P(r - r_0) = 1 \quad (\text{B.21})$$

where

$$P = \frac{1}{r_0^T Q r_0 - F} Q \quad (\text{B.22})$$

$$p = q / (r0' * q * r0 - F);$$

Now diagonalize matrix P into $P = RDR^T$, with R orthogonal and D diagonal.

The formulas are

$$R = \begin{bmatrix} \cos(\theta) & -\sin(\theta) \\ \sin(\theta) & \cos(\theta) \end{bmatrix} \quad (\text{B.23})$$

where

$$\theta = \frac{1}{2} \tan^{-1} \left(\frac{2P_{12}}{P_{11} - P_{22}} \right) \quad (\text{B.24})$$

The diagonal entries of D are

$$D_{11} = \frac{1}{2}(P_{11} + P_{22}) + \frac{1}{2}(P_{11} - P_{22}) \cos(2\theta) + P_{12} \sin(2\theta) \quad (\text{B.25})$$

$$D_{22} = \frac{1}{2}(P_{11} + P_{22}) - \frac{1}{2}(P_{11} - P_{22}) \cos(2\theta) - P_{12} \sin(2\theta) \quad (\text{B.26})$$

```
% The rotation matrix R and the diagonal D can be calculated
% analytically using equation 29 to 32, or just by calculating
% the eigenvalues of p using the command eig(). This retruns
% eigenvectors and can be split into [R, D].
% The second method is more efficient and compact.
```

$$[R, D] = \text{eig}(p);$$

$$D11 = D(1,1);$$

$$D22 = D(2,2);$$

Finally, define the vector z by $r = r_0 + Rz$, then it follows

$$x^T D x = 1$$

i.e.

$$D_{11}x_1^2 + D_{22}x_2^2 = 1$$

Its solution leads to the parameterization of r . The solution is

$$z = \begin{bmatrix} \frac{1}{\sqrt{D_{11}}} \cos(\phi) \\ \frac{1}{\sqrt{D_{22}}} \sin(\phi) \end{bmatrix}$$

```
theta = linspace(0, 2 * pi, 1000);
z = [cos(theta) / sqrt(D11);
      sin(theta) / sqrt(D22)];
```

Then, from above,

$$r = r_0 + Rz$$

```
r = r0 + R * z;
rx = r(1,:);
ry = r(2,:);
```

Inspecting this equation, one realizes that the semi-axes of the ellipse are the columns of R , but scaled by $\frac{1}{\sqrt{D_{11}}}$ and $\frac{1}{\sqrt{D_{22}}}$.

```
a1 = 1 / sqrt(D11);
a2 = 1 / sqrt(D22);

semi_major = max(a1, a2);
semi_minor = min(a1, a2);
```

```
end
```

You may choose to find the minimum area ellipse among all possible ellipses, and this is easily achievable because the ellipses are a function of a single variable t . Using a function minimizer, the critical value of t that minimizes the ellipse area can be found.

```
% Earlier in the code this was used to find the minimum single variable t
% to calculate the ellipse with the minimum area.

% Opp_function = @(t) ellipsoppvervlak(V + t * W);
% t_optimaal = fminbnd(Opp_function, t1, t2);
% a = transpose(V + t_optimaal * W);

function Opp = ellipsoppvervlak(a)
A = 1; B = a(1); C = a(2); D = a(3); E = a(4); F = a(5);
q = [A, B/2;
      B/2, C];
G = [D;
      E];
r0 = -(0.5) * (q^-1) * G; % center ellips
p = q / (transpose(r0) * q * r0 - F);
[~, D] = eig(p);
D11 = D(1,1);
D22 = D(2,2);
a = 1 / (sqrt(D11));
b = 1 / (sqrt(D22));
Opp = pi * a * b;
end
```

C

Spread of Individual Impact Angle Measurements

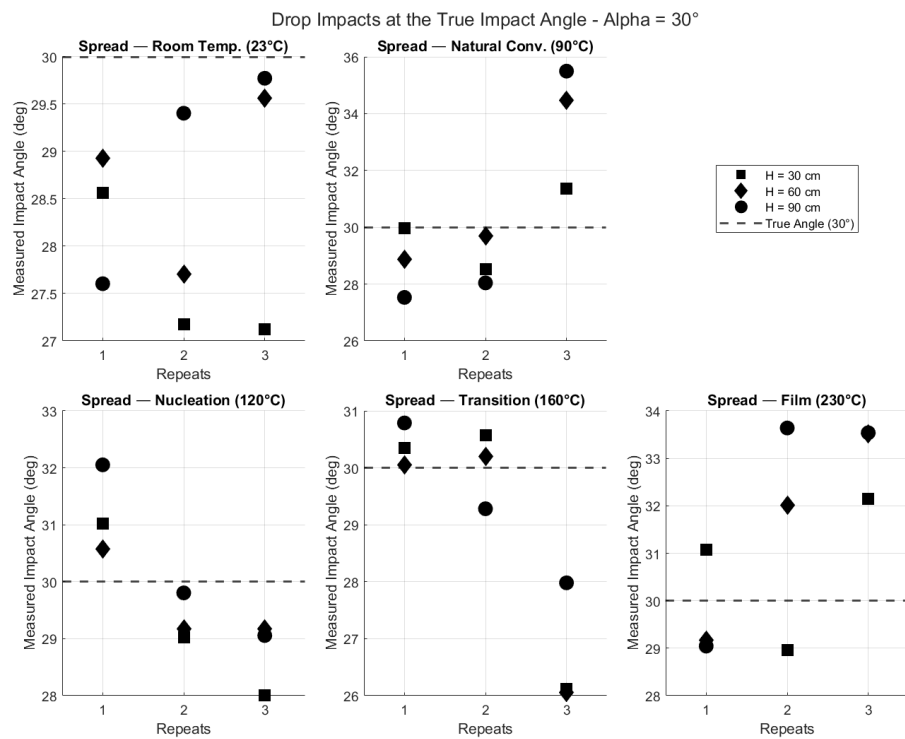


Figure C.1: The spread of the measured impact angle at $\alpha = 30^\circ$ ($\theta = 60^\circ$) with three different drop heights. Each data point is an average of 3 blood drops ($N = 3$). It seems that the drop height (i.e. the impact velocity) does not affect the accuracy of the impact angle.

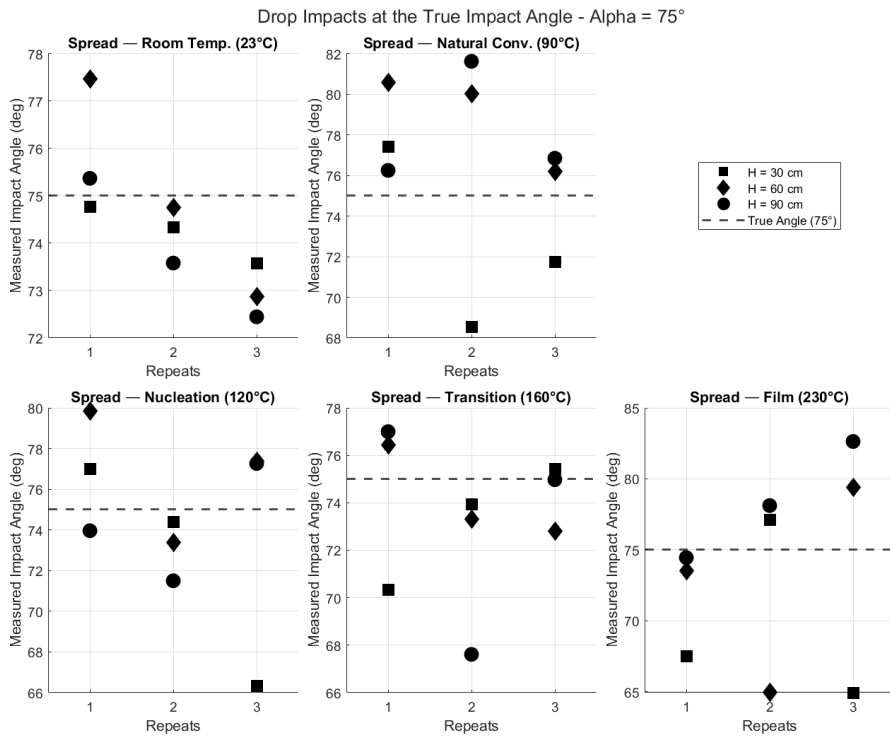


Figure C.2: The spread of the measured impact angle at $\alpha = 75^\circ$ ($\theta = 15^\circ$) with three different drop heights. Each data point is an average of 3 blood drops ($N = 3$). It seems that the drop height (i.e. the impact velocity) does not affect the accuracy of the impact angle.

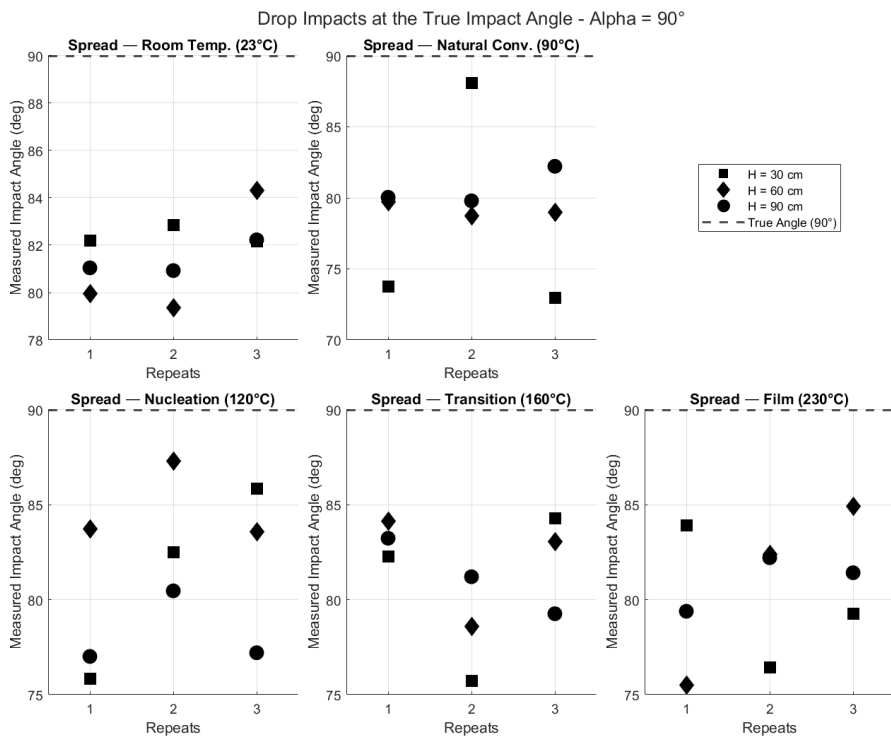


Figure C.3: The spread of the measured impact angle at $\alpha = 90^\circ$ ($\theta = 0^\circ$) with three different drop heights. Each data point is an average of 3 blood drops ($N = 3$). It seems that the drop height (i.e. the impact velocity) does not affect the accuracy of the impact angle.

D

Bloodstain graphs

Room Temperature

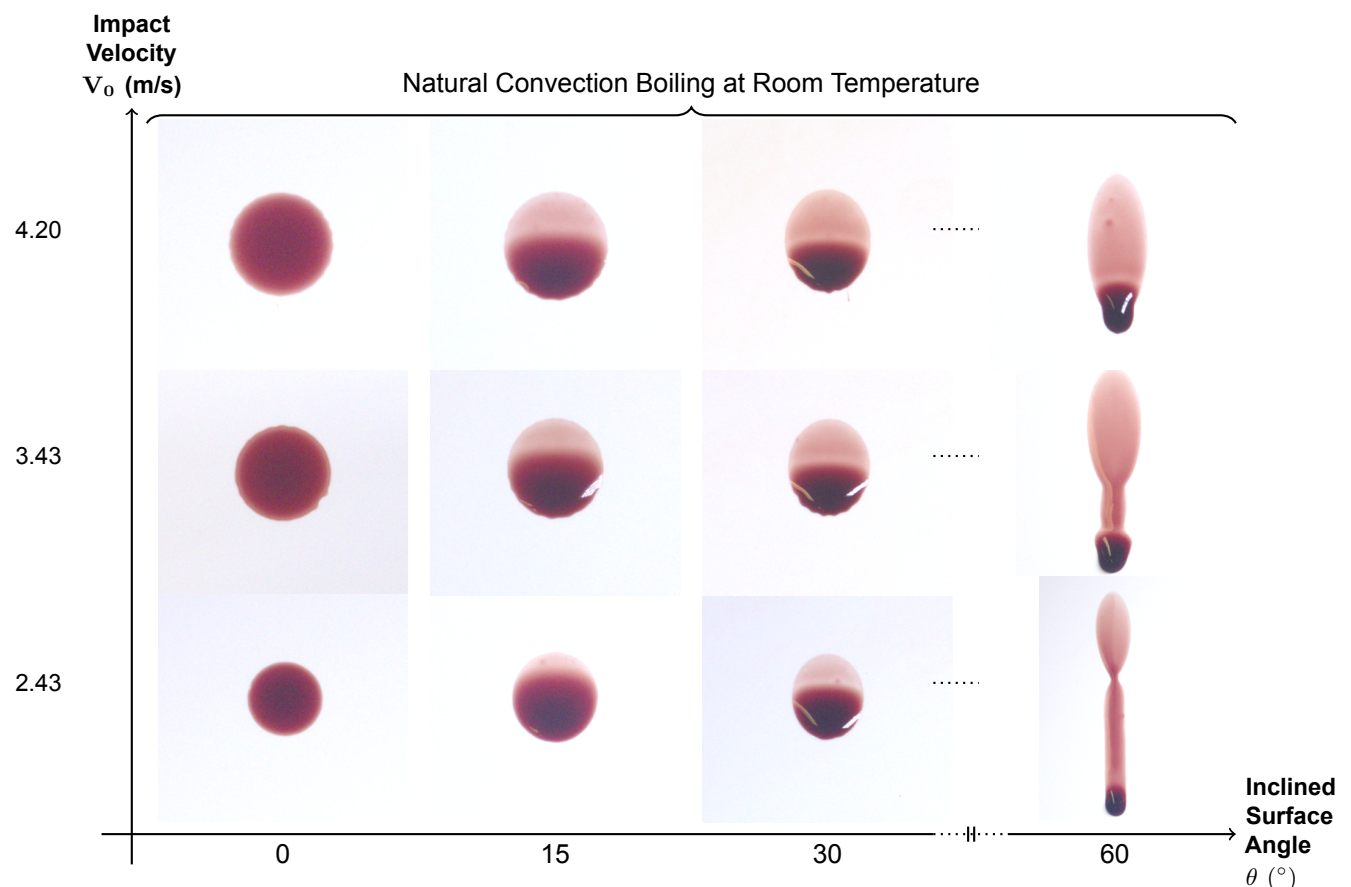


Figure D.1: Recorded pictures 45 seconds after impact of the passive drip stains on a specific surface temperature. In this figure the surface was $\sim 23^{\circ}\text{C}$ (Repeat 1).

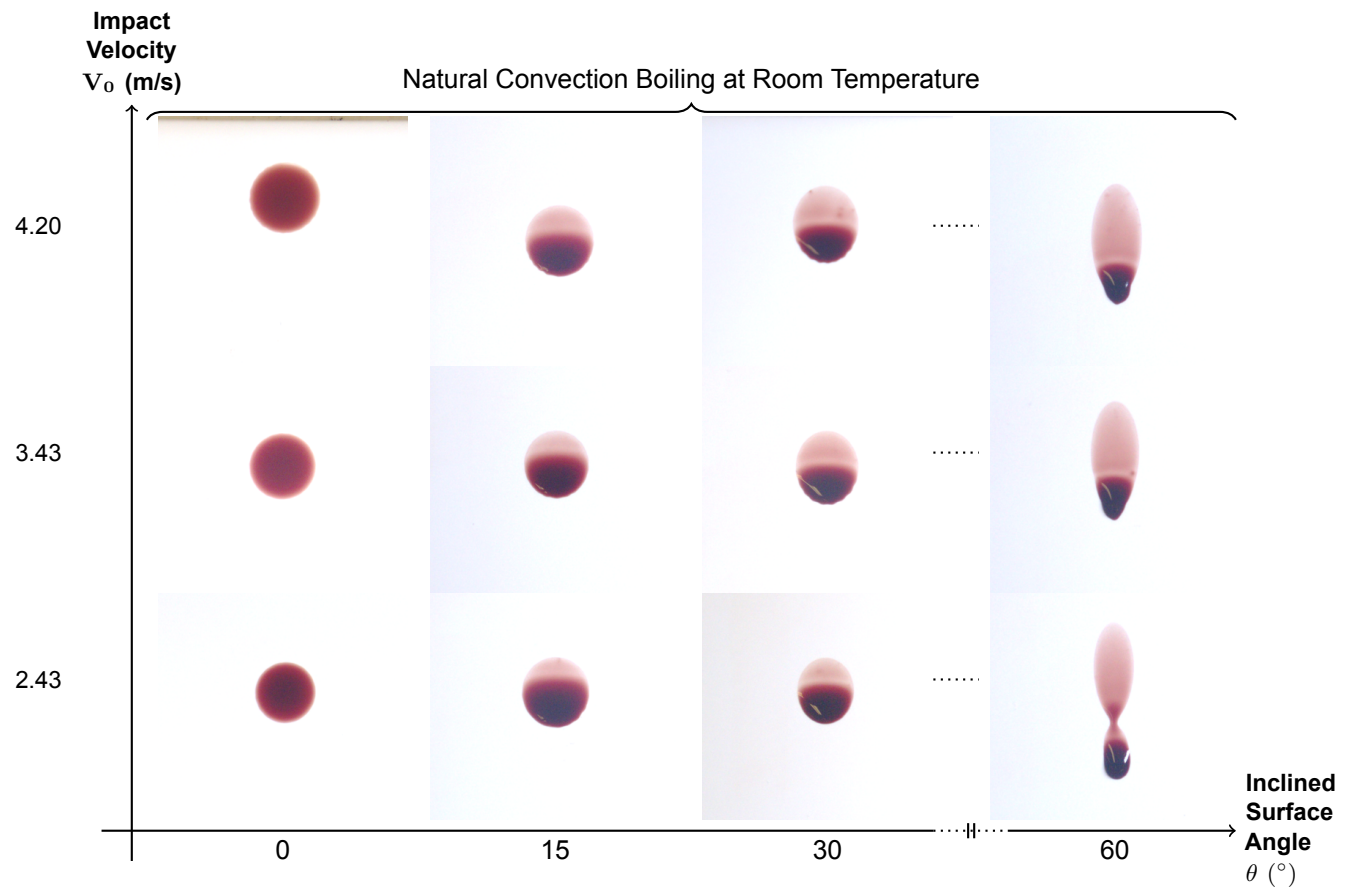


Figure D.2: Recorded pictures 45 seconds after impact of the passive drip stains on a specific surface temperature. In this figure the surface was $\sim 23^\circ C$ (Repeat 3).

Natural Convection Boiling

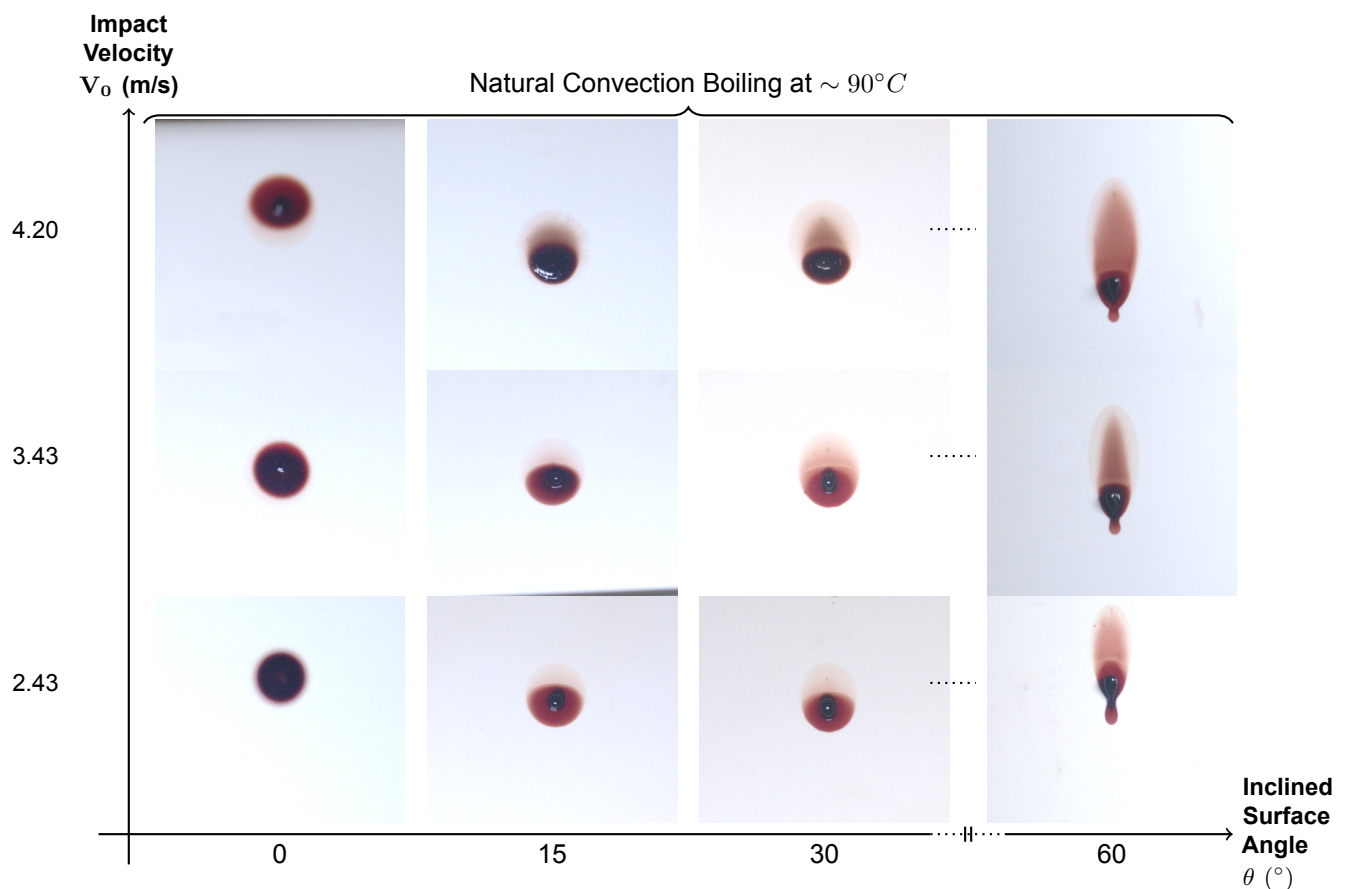


Figure D.3: Recorded pictures 45 seconds after impact of the passive drip stains on a specific surface temperature. In this figure the surface was $\sim 90^\circ C$ (Repeat 1).

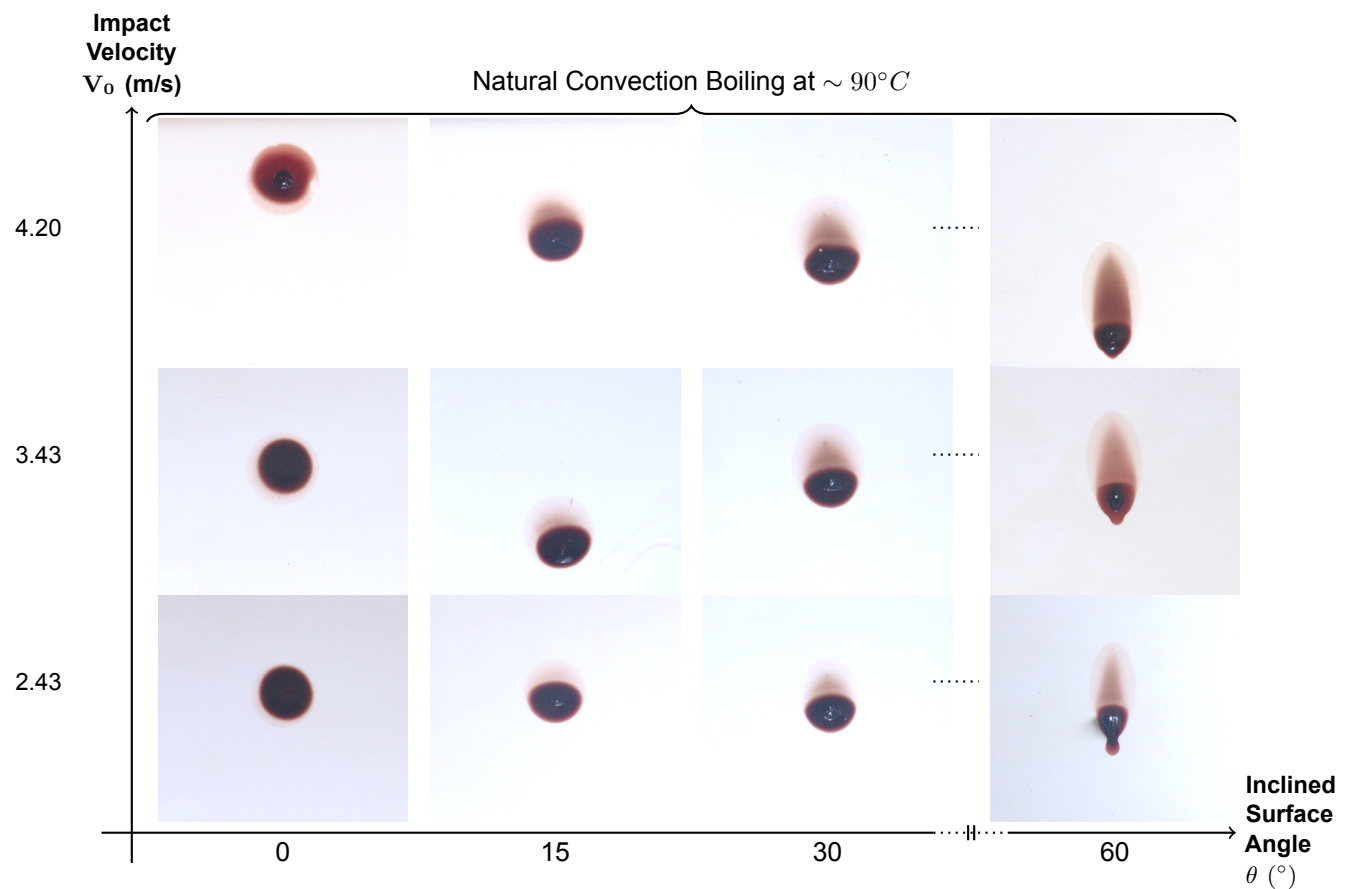


Figure D.4: Recorded pictures 45 seconds after impact of the passive drip stains on a specific surface temperature. In this figure the surface was $\sim 90^\circ C$ (Repeat 3).

Nucleate Boiling

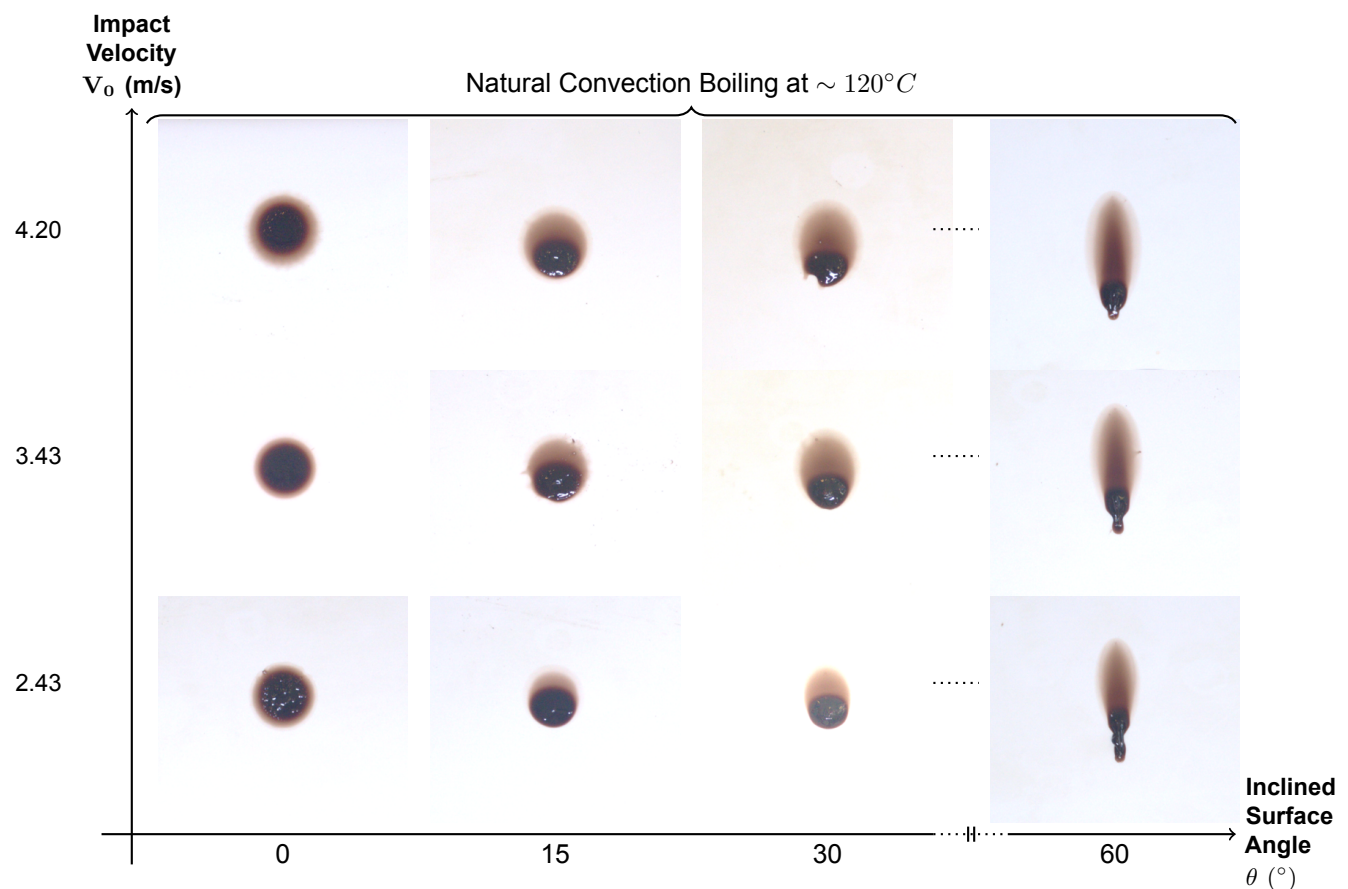


Figure D.5: Recorded pictures 45 seconds after impact of the passive drip stains on a specific surface temperature. In this figure the surface was at room temperature $\sim 120^{\circ}C$ (Repeat 1).

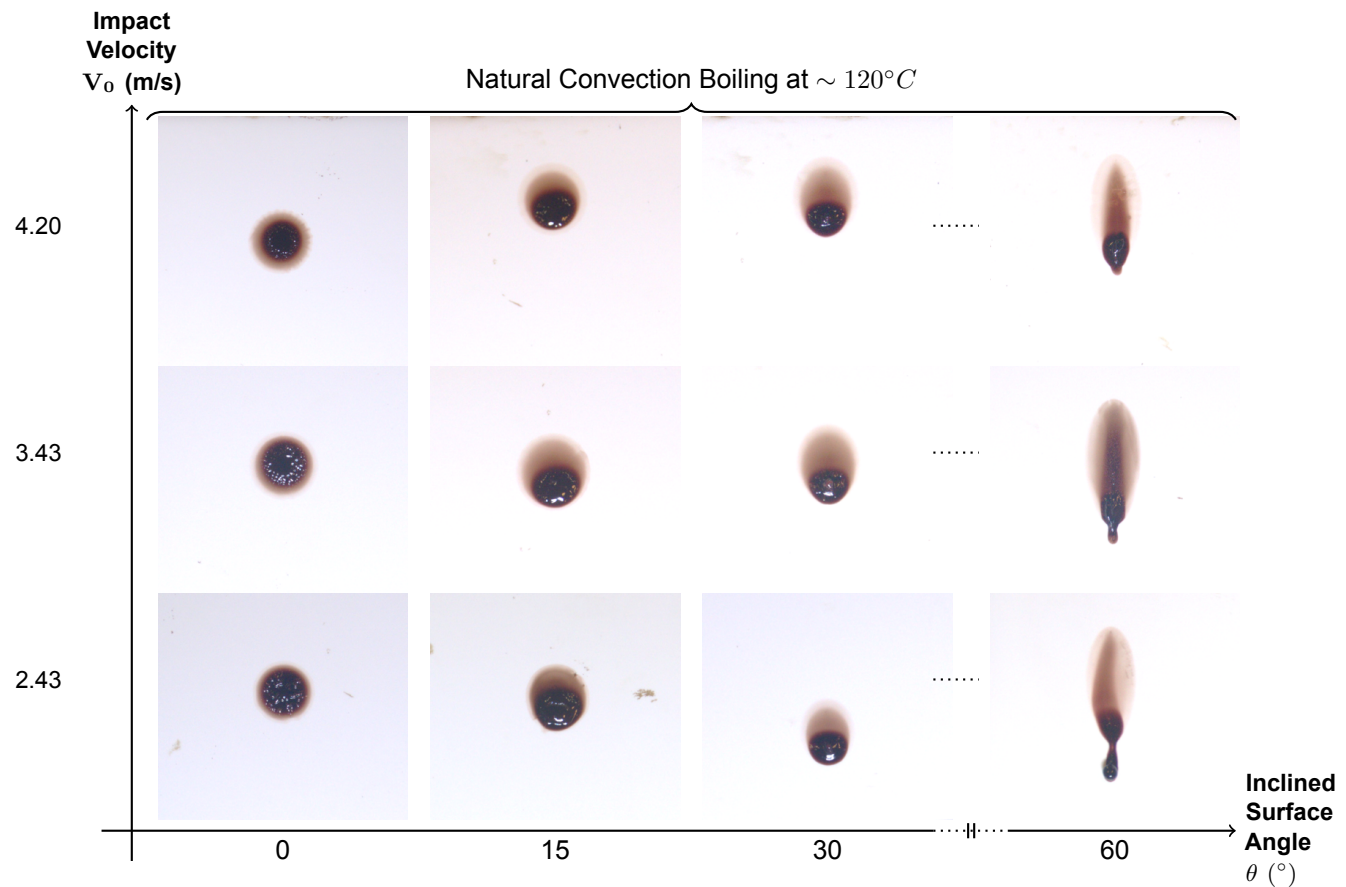


Figure D.6: Recorded pictures 45 seconds after impact of the passive drip stains on a specific surface temperature. In this figure the surface was at room temperature $\sim 120^\circ C$ (Repeat 3).

Transition Boiling

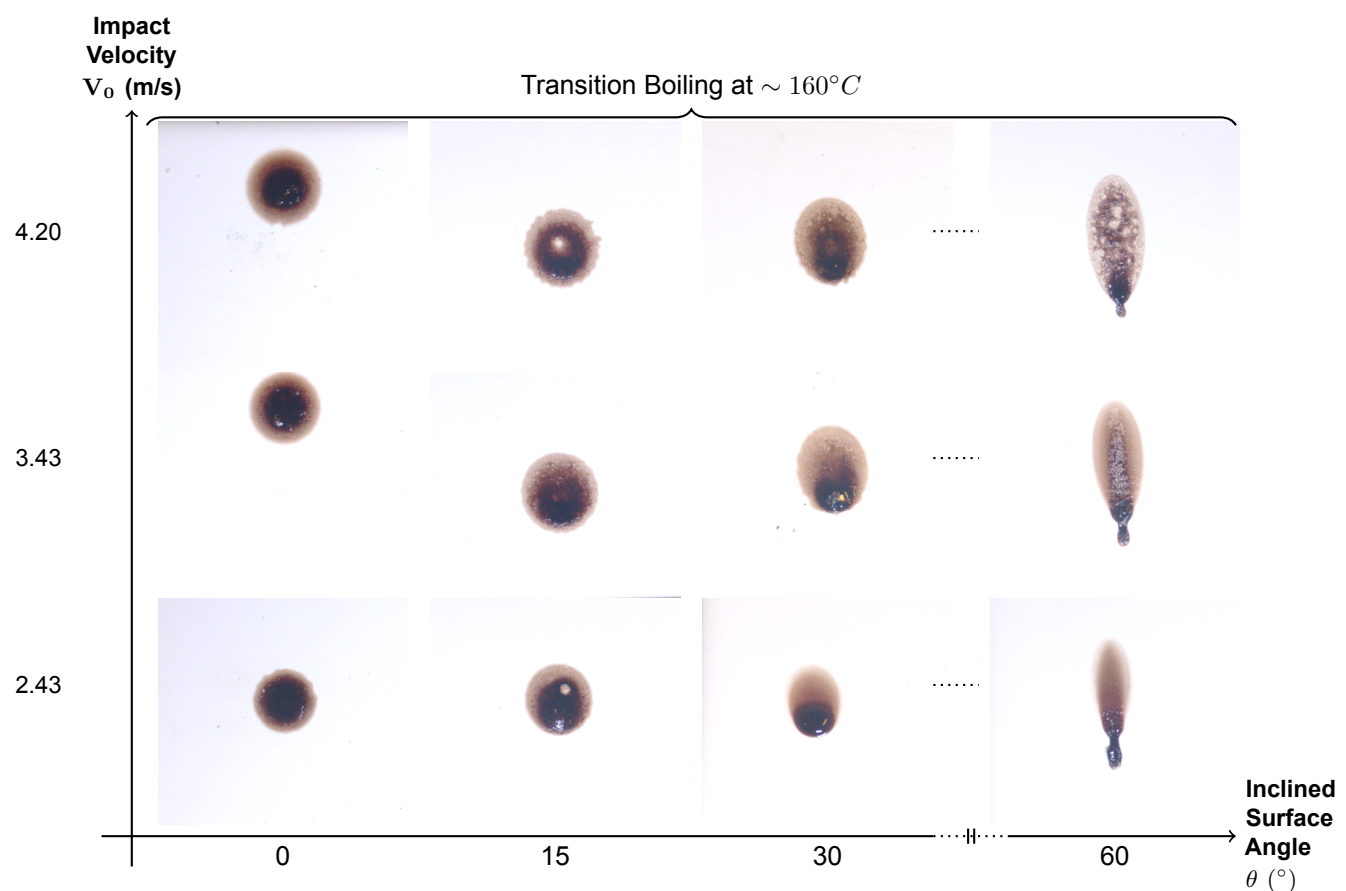


Figure D.7: Recorded pictures 45 seconds after impact of the passive drip stains on a specific surface temperature. In this figure the surface was heated to a temperature of $\sim 160^{\circ}C$ (Repeat 2).

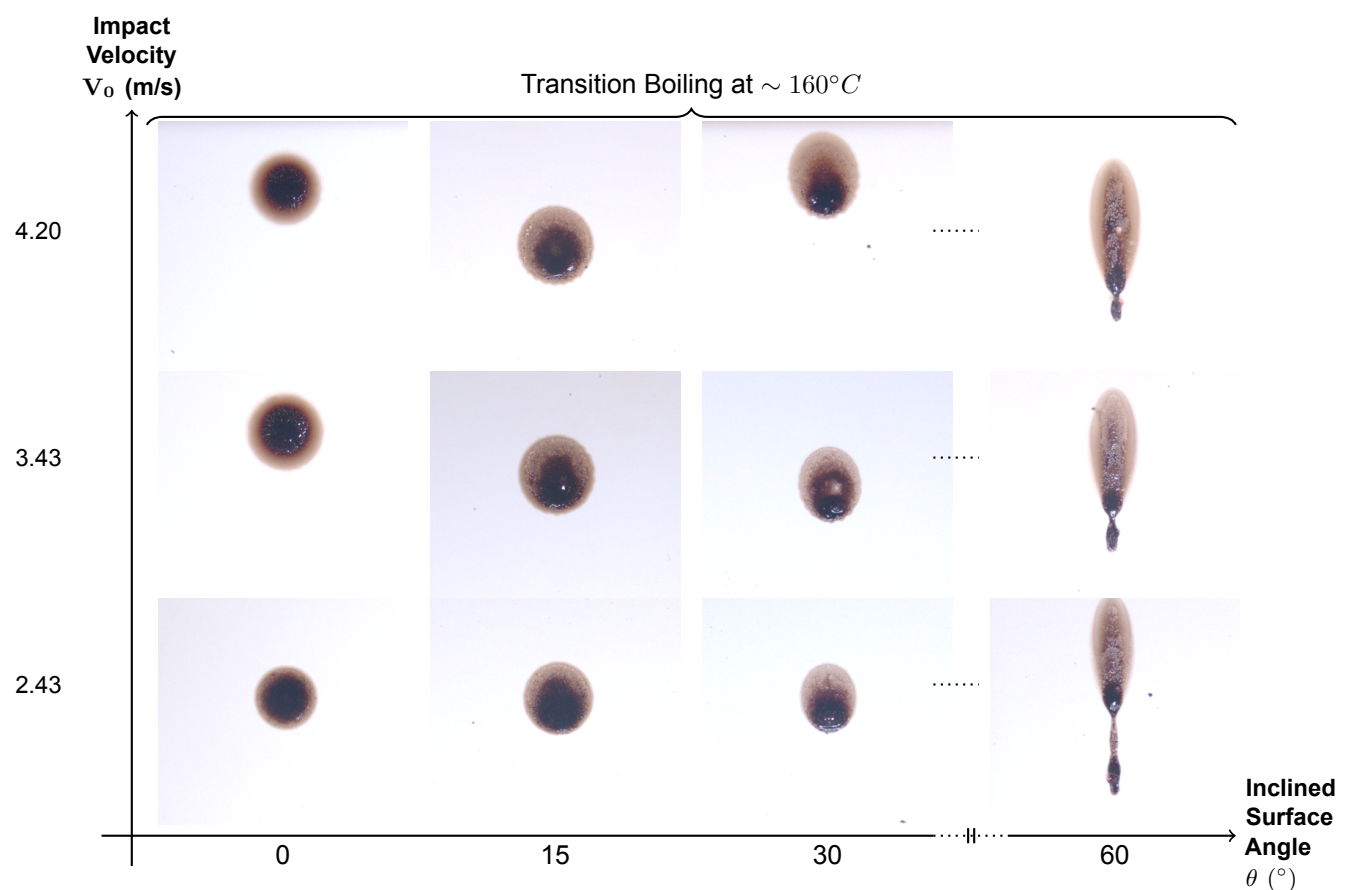


Figure D.8: Recorded pictures 45 seconds after impact of the passive drip stains on a specific surface temperature. In this figure the surface was heated to a temperature of $\sim 160^{\circ}C$ (Repeat 3).

Film Boiling

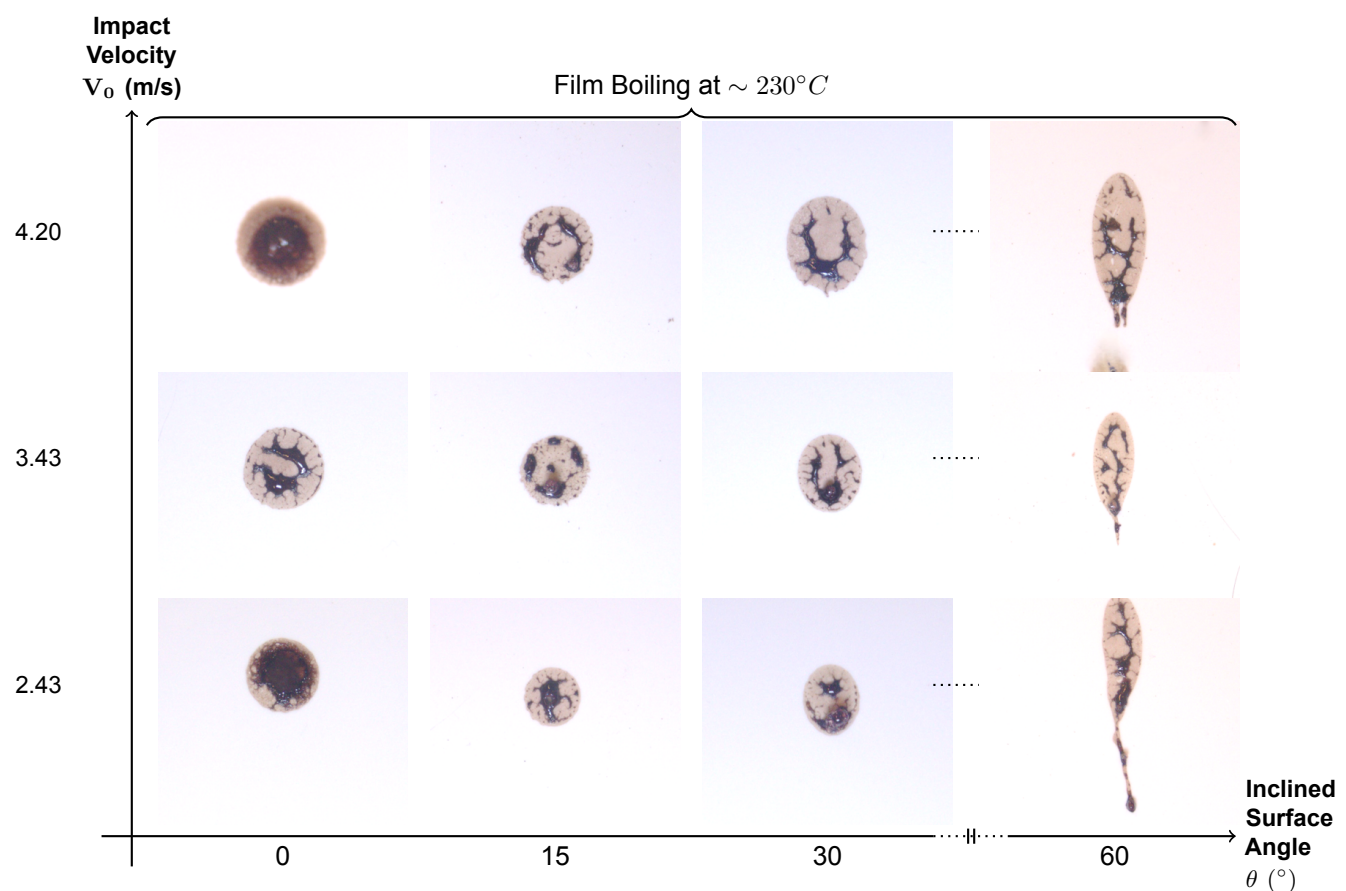


Figure D.9: Recorded pictures 45 seconds after impact of the passive drip stains on a specific surface temperature. In this figure the surface was heated to a temperature of $\sim 230^\circ C$ (Repeat 1).

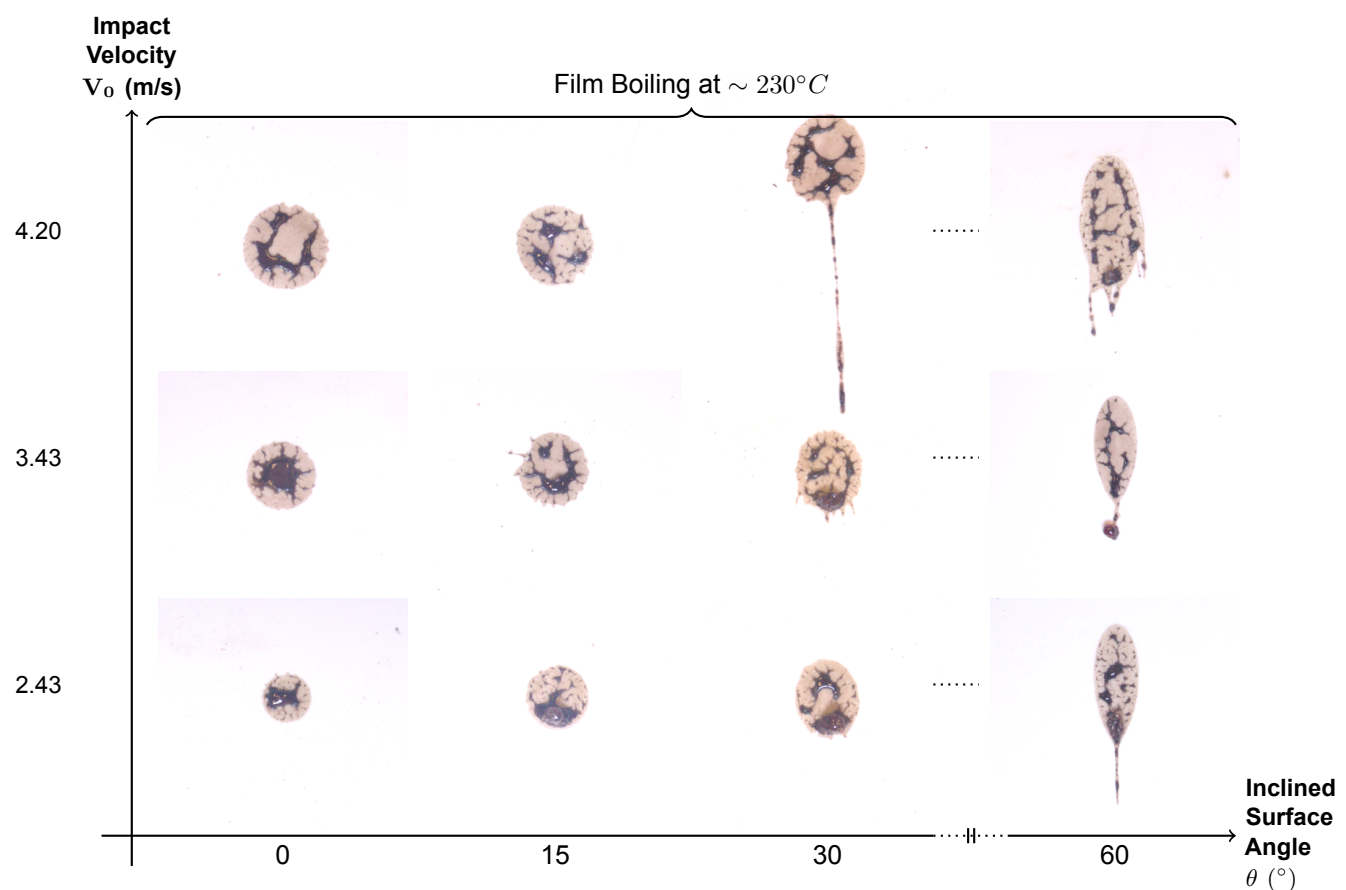
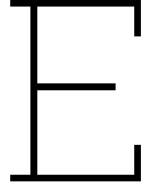


Figure D.10: Recorded pictures 45 seconds after impact of the passive drip stains on a specific surface temperature. In this figure the surface was heated to a temperature of $\sim 230^{\circ}C$ (Repeat 2).



Used equations

Impact angle

In general, the impact angle is calculated by using Equation E.1. With the assumption that this equation still holds for the bloodstain that has been analyzed.

$$\sin \alpha = (W_{max}/L_{max}) \quad (\text{E.1})$$

Differentiating both sides of Equation E.1 implicitly with respect to W/L gives:

$$\cos \alpha \cdot \frac{d(\alpha)}{d(W/L)} = 1 \quad (\text{E.2})$$

rewriting,

$$d(\alpha) = \frac{1}{\cos \alpha} \cdot d(W/L). \quad (\text{E.3})$$

This mathematical interpretation implies that for almost circular bloodstains, Equation E.1 does not accurately estimates the impact angle α .

Drop impact

$$We = \frac{\rho D_0 V_0^2}{\sigma} \quad (\text{E.4})$$

$$Re = \frac{\rho D_0 V_0}{\mu} \quad (\text{E.5})$$

$$\frac{D_{max}}{D_0} \cdot Re^{-1/5} = \frac{P^{1/2}}{A + P^{1/2}} \quad (\text{E.6})$$

In Equation E.6, the parameter P , referred to as the *impact parameter*, is defined as

$$P = We Re^{-2/5}.$$

The constant A is a fitting parameter, with a value of

$$A = 1.24 \pm 0.01.$$

$$\frac{W_{max}}{D_0} = Re^{1/5} \cdot \frac{P^{1/2} \sin \alpha}{(A + P^{1/2}(\sin \alpha)^{4/5})} \quad (\text{E.7})$$

Impact velocity and the initial droplet diameter

$$V_0(h) = \sqrt{2gh} \quad (\text{Bernoulli/conservation of energy}) \quad (\text{E.8})$$

$$\mathcal{V} = \frac{4}{3}\pi \left(\frac{D_0}{2}\right)^3 \Rightarrow D_0 = \left(\frac{6\mathcal{V}}{\pi}\right)^{1/3} \quad (\text{E.9})$$

F

Task Division

Distribution of the workload for writing the report

Table F.1: Distribution of the workload

Task	Student Name(s)
Preface	K. Karkus
Samenvatting	
Summary	
Chapter 1 Introduction	K. Karkus
Chapter 2 Theory	2.1: M. Kortlever; 2.2 - 2.4: M. Bouwman
Chapter 3 Experimental Methods	3.1: K. Karkus; 3.2: J. Wolberink & M. Bouwman; 3.3 - 3.6: M. Bouwman
Chapter 4 Results and Interpretation	4.1: M. Bouwman; 4.2: K. Karkus, M. Kortlever, J. Wolberink; 4.3 - 4.4: M. Bouwman
Chapter 5 Discussion	
Chapter 6 Conclusion	
Chapter 7 Recommendations and Outlook	
Appendix A, B, C, D, E	M. Bouwman
Editors	M. Bouwman, K. Karkus, M. Kortlever & J. Wolberink
CAD and Figures	M. Bouwman
Document Design and Layout	M. Bouwman

Task allocation

This project is carried out by three- and one fourth-year student with in total three different backgrounds. In the group agreement contract, all roles and tasks are defined. The table below gives a summary of the roles and task distribution.

Table F.2: Table with a summary of all the roles and tasks.

Name	Study	Role	Task(s)	Timeline
Kuba Karkus	FO Forensisch Onderzoek (Forensic Investigation)	Vice-chair	<ul style="list-style-type: none"> • Running experiments containing blood • Planning of experiments • Communicating with group members while they're not present • Providing literature research from the forensic point of view 	Can be switched during the project
Mees Bouwman	TN Technische Natuurkunde (Applied Physics)	Chair	<ul style="list-style-type: none"> • Taking the lead in literature research on the necessary mathematics and physics • Designing the experimental setup and measure methods • Administrator Overleaf (LaTeX) documentation • Data-analysis 	Can be switched during the project
Mariëlle Kortlever	FO Forensisch Onderzoek (Forensic Investigation)	Note taker	<ul style="list-style-type: none"> • Running experiments containing blood • Planning of experiments • Compiling of literature research 	Can be switched during the project
Jimme Wolberink	ARC Archeologie (Archaeology)	Planner	<ul style="list-style-type: none"> • Taking care of visual presentation • Camera work • Designing the research strategy 	Can be switched during the project